Cell Reports

Article

PRMT2-mediated upregulation of miR-323-3p in sensory neurons promotes trigeminal neuropathic pain by targeting Kv2.1 channels

Graphical abstract

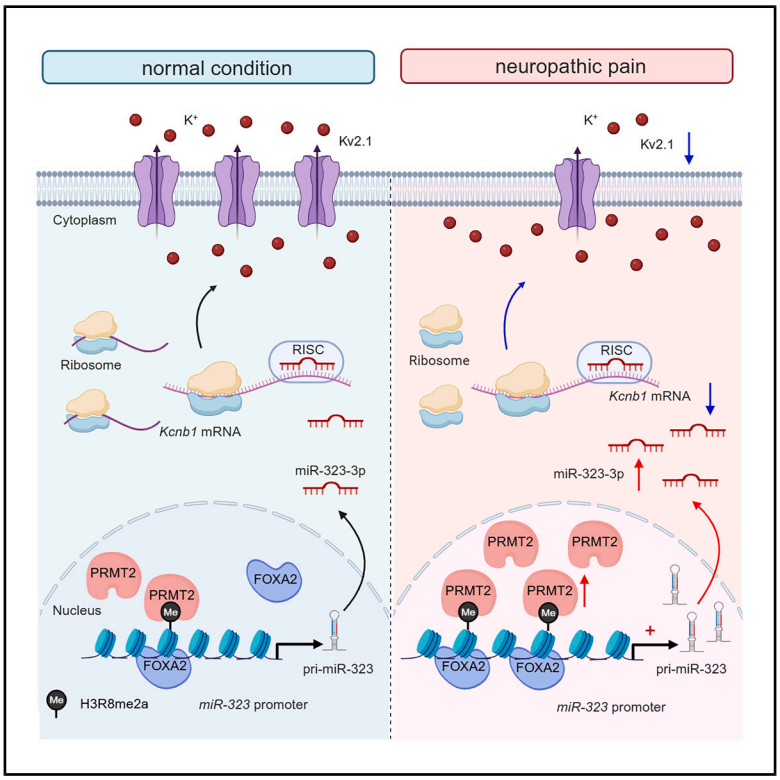

Highlights

- miR-323-3p is the most upregulated microRNA in injured TG neurons
- The transcription factor FOXA2 promotes miR-323-3p expression
- PRMT2-mediated H3R8me2a increases the binding of FOXA2 to miR-323-3p
- miR-323-3p regulates nociceptive behaviors in rats by targeting Kv2.1 channels

Authors

Renfei Qi, Yu Tao, Shoupeng Wang, ..., Yuan Zhang, Yongjun Rui, Jin Tao

Correspondence

yuanzhang@suda.edu.cn (Y.Z.), ruiyongjun@suda.edu.cn (Y.R.), taoj@suda.edu.cn (J.T.)

In brief

Qi et al. report a critical role of the PRMT2/FOXA2/miR-323-3p/Kv2.1 signaling axis in sensory neurons that contributes to TG neuronal hyperexcitability and trigeminal-mediated neuropathic pain in rats. This mechanistic understanding may enable the discovery of potential therapeutic targets for neuropathic pain management.

Qi et al., 2025, Cell Reports *44*, 116028
August 26, 2025
https://doi.org/10.1016/j.celrep.2025.116028

CellPress

Cell Reports

CellPress
OPEN ACCESS

Article

PRMT2-mediated upregulation of miR-323-3p in sensory neurons promotes trigeminal neuropathic pain by targeting Kv2.1 channels

Renfei Qi,[1,2,7] Yu Tao,[2,7] Shoupeng Wang,[2,7] Yueting Zhou,[2] Yufang Sun,[2] Dongsheng Jiang,[3,6] Zitong Huang,[2] Gang Chen,[4] Gang Zhao,[1] Yuan Zhang,[5,*] Yongjun Rui,[1,*] and Jin Tao[2,8,*]

[1]Orthopaedic Institute, Wuxi Ninth People's Hospital Affiliated to Soochow University, Wuxi 214062, P.R. China
[2]Jiangsu Key Laboratory of Drug Discovery and Translational Research for Brain Diseases, Centre for Ion Channelopathy, School of Basic Medical Sciences, Suzhou Medical College of Soochow University, Suzhou 215123, P.R. China
[3]Precision Research Center for Refractory Diseases, Shanghai General Hospital, Shanghai Jiao Tong University, Shanghai 201620, P.R. China
[4]Department of Neurosurgery, The First Affiliated Hospital of Soochow University, Suzhou 215006, P.R. China
[5]Clinical Research Center of Neurological Disease, Department of Geriatrics, The Second Affiliated Hospital of Soochow University, Suzhou 215004, P.R. China
[6]Institute of Regenerative Biology and Medicine, Helmholtz Zentrum München, 81377 Munich, Germany
[7]These authors contributed equally
[8]Lead contact
*Correspondence: yuanzhang@suda.edu.cn (Y.Z.), ruiyongjun@suda.edu.cn (Y.R.), taoj@suda.edu.cn (J.T.)
https://doi.org/10.1016/j.celrep.2025.116028

SUMMARY

Herein, we show a molecular pathway driven by an evolutionarily conserved microRNA (miRNA) in sensory neurons to control neuropathic pain. By employing high-throughput sequencing analysis, we find that miRNA-323-3p (miR-323-3p) exhibits the most significant upregulation in injured trigeminal ganglia (TGs). Local inhibition of miR-323-3p in injured TGs suppresses established trigeminal neuropathic pain but has no effect on inflammatory pain. Mechanistically, nerve injury upregulates the protein expression of protein arginine methyltransferase 2 (PRMT2), which promotes asymmetric dimethylation of H3R8, thereby facilitating the binding of the transcription factor forkhead box A2 (FOXA2) to the miR-323-3p promoter and resulting in the upregulation of miR-323-3p expression. Furthermore, the increased miR-323-3p expression induces significant reductions in Kv2.1 protein expression and channel currents, resulting in TG neuronal hyperexcitability. Conversely, the downregulation of miR-323-3p in injured TGs restores the decreased Kv2.1 expression and attenuates nerve-injury-induced mechanical hypersensitivity. The PRMT2/FOXA2/miR-323-3p/Kv2.1 signaling axis in sensory neurons may offer therapeutic targets in neuropathic pain management.

INTRODUCTION

Neuropathic pain caused by somatosensory nerve damage or disease is a common type of chronic pain that has a major impact on quality of life.[1,2] Current analgesics, including nonsteroidal anti-inflammatory drugs (NSAIDs) and opioids, often lack efficacy or have notable side effects in most patients with neuropathic pain; thus, the therapeutic management of this disorder is difficult.[3] Therefore, understanding the cellular and molecular mechanisms underlying neuropathic pain is crucial for the development of cutting-edge therapies for this condition. Accumulating studies in first-order sensory neurons, such as trigeminal ganglion (TG) neurons, have shown that peripheral nerve injury can cause alterations in gene expression profiles associated with neuropathic pain at both the transcriptional and translational levels.[4,5] These changes may affect some key genomic signatures/regulatory processes and result in the initiation and maintenance of neuropathic pain.[4–6] Elucidation of the molecular mechanisms through which these changes occur in TGs following nerve injury may open avenues for the development of innovative approaches to manage neuropathic pain.

MicroRNAs (miRNAs) are short noncoding RNAs that play a crucial role in the post-transcriptional regulation of gene expression by binding to the 3′ UTRs of target mRNAs.[7,8] Abnormal expression of miRNAs has been observed in various human disorders, including neuropathic pain. This finding suggests that miRNAs may have potential as therapeutic targets or diagnostic markers for neuropathic pain and related conditions.[9] Notably, the regulation of miRNA expression has been investigated as a promising therapeutic approach,[10] leading to ongoing preclinical and clinical investigations of miRNA-based therapies.[11] miRNA-323-3p (miR-323-3p), which is abundantly expressed and well

conserved across species, has been demonstrated to participate in a variety of biological processes, including oxidative stress and the pathogenesis of several diseases, including glioblastoma and ectopic pregnancy.[12,13] Furthermore, suppressing miR-323-3p can inhibit vascular endothelial cell apoptosis in coronary heart disease by upregulating the expression of sirtuin-1.[14] Although limited studies have demonstrated a functional regulatory contribution of miR-323-3p to neurological disorders, miR-323-3p has recently been shown to regulate receptor protein-tyrosine kinase erbB-4 and is involved in depression.[15] However, it remains to be determined whether and how miR-323-3p participates in regulating the sensory processing of neuropathic pain behaviors.

In the current study, we elucidated a critical role of the protein arginine methyltransferase 2 (PRMT2)/forkhead box A2 (FOXA2)/miR-323-3p/Kv2.1 signaling axis in TG neurons contributing to trigeminal neuropathic pain. Nerve injury induces the upregulation of PRMT2, which promotes asymmetric dimethylation of histone H3 arginine 8 (H3R8me2a), thereby facilitating the binding of the FOXA2 transcription factor (TF) to the *miR-323-3p* promoter and resulting in the upregulation of *miR-323-3p* expression. We also revealed that the increased expression of miR-323-3p contributed to the onset and maintenance of nerve-injury-induced neuropathic pain by targeting the Kv2.1 potassium (K^+) channel. This mechanistic understanding may facilitate the discovery of therapeutic strategies to manage neuropathic pain.

RESULTS

miR-323-3p is upregulated in TG neurons after CCI-ION

A unilateral chronic constriction injury (CCI) of the infraorbital nerve (ION) was used to establish a model of trigeminal neuropathic pain. Rats exhibited a dramatic decrease in the mechanical response threshold for escape behavior (escape threshold) at 14, 21, and 28 days following CCI-ION operation compared with that of the sham groups (Figure 1A). We therefore performed RNA sequencing (RNA-seq) on the injured TGs 14 days post-CCI-ION (Database: GSE192803). Among the twenty-seven miRNAs with elevated expression levels in the TGs, ten miRNAs showed high conservation across species, including humans and rats (Figure 1B). Subsequently, their expression in the TGs was validated using qPCR analysis. Specifically, the expression of six miRNAs—miR-146a-5p, miR-21-5p, miR-221-3p, miR-323-3p, miR-342-3p, and miR-370-3p—was significantly elevated in the injured TGs following CCI-ION. Notably, miR-323-3p showed the greatest increase, with an approximate 285% elevation compared to the sham group (Figure 1C). Thus, we performed a comprehensive analysis of the expression and functional characteristics of miR-323-3p. We observed a high abundance of the miR-323-3p transcript specifically within the TGs by qPCR analysis (Figures 1D and S1), and miR-323-3p transcript abundance in the TGs was even higher than that in the brain (~3.1-fold; Figure 1E). Moreover, we examined the time course of miR-323-3p expression in the ipsilateral TGs following CCI-ION. qPCR analysis demonstrated that the miR-323-3p level was markedly increased on day 14 and remained high for at least 28 days in the rats subjected to CCI-ION, while the miR-323-3p expression level remained unchanged in the sham-operated rats throughout the experimental period (Figure 1F). Furthermore, we examined miR-323-3p expression in a model of inflammatory pain, which is a distinct subchronic pain syndrome with partially overlapping molecular mechanisms compared to neuropathic pain,[16] and found that the expression level of miR-323-3p in the TGs was unaltered following CFA-induced inflammatory pain (Figure 1G). Next, we examined the cellular distribution of miR-323-3p in the TGs. Fluorescence *in situ* hybridization (FISH) assays demonstrated that miR-323-3p exhibited basal expression in both small- and medium-sized neurons, and miR-323-3p expression was increased 14 days following CCI-ION operation (Figure 1H). The combination of FISH and immunofluorescence staining (immunoFISH) showed that miR-323-3p was predominantly coexpressed with the neuronal marker NeuN but was rarely coexpressed with the satellite glial cell-specific marker GS (Figure 1I). Quantitative analysis showed that approximately 96.6% of the miR-323-3p$^+$ cells were NeuN$^+$, whereas only ~4.6% coexpressed GS (Figure 1J), indicating that miR-323-3p is primarily expressed in TG neurons.

miR-323-3p regulates nociceptive behaviors

To assess miR-323-3p's role in trigeminal neuropathic pain, we injected miR-323-3p antagomir (antagomir-323) or negative control (antagomir-NC) unilaterally into the TG on day 14 post-CCI-ION. qPCR analysis confirmed a significant decrease in miR-323-3p expression levels in TGs following antagomir-323 treatment (Figure S2A). As depicted in Figure 2A, administration of antagomir-323 by intra-TG injection dramatically attenuated CCI-ION-induced mechanical hypersensitivity, while administration of antagomir-NC did not result in these effects (Figure 2A). This was evidenced by an increase in the escape threshold to mechanical stimulation from day 2 to day 3 following drug administration in both male rats (Figure 2A) and female rats (Figure 2B). Subsequently, we further employed a recombinant lentiviral vector, lenti-hSyn-miR-323-3p-antisense (miR-323-AS), which contained an EGFP construct serving as an expression marker (Figure S2B), to examine the effect of miR-323-3p blockade on neuropathic pain behaviors. After injection of miR-323-AS, the expression of EGFP was observed on day 3 and persisted until day 21 (Figure S2C). The application of miR-323-AS at 14 days after CCI-ION significantly ameliorated mechanical hypersensitivity from day 3 to day 7 following drug administration (Figure 2C). Additionally, we investigated the role of miR-323-3p in the development of chronic neuropathic pain by administering miR-323-AS prior to CCI-ION. Compared to the sham surgery, preinjection of miR-323-AS significantly reduced the extent of mechanical hypersensitivity induced by CCI-ION on day 14 after surgery (Figure 2D). However, the administration of miR-323-AS did not alleviate inflammatory pain (Figure 2E), suggesting that miR-323-3p may specifically play a functional role in neuropathic pain. Subsequently, we investigated whether mimicking the upregulation of miR-323-3p observed in TG neurons following CCI-ION in naive rats affects nociceptive behaviors. Administration of an miR-323-3p agomir (agomir-323) resulted in the induction of mechanical pain hypersensitivity (Figure 2F), while administration of the NC agomir (agomir-NC) did not elicit a similar response. Furthermore, we utilized a lentiviral approach to

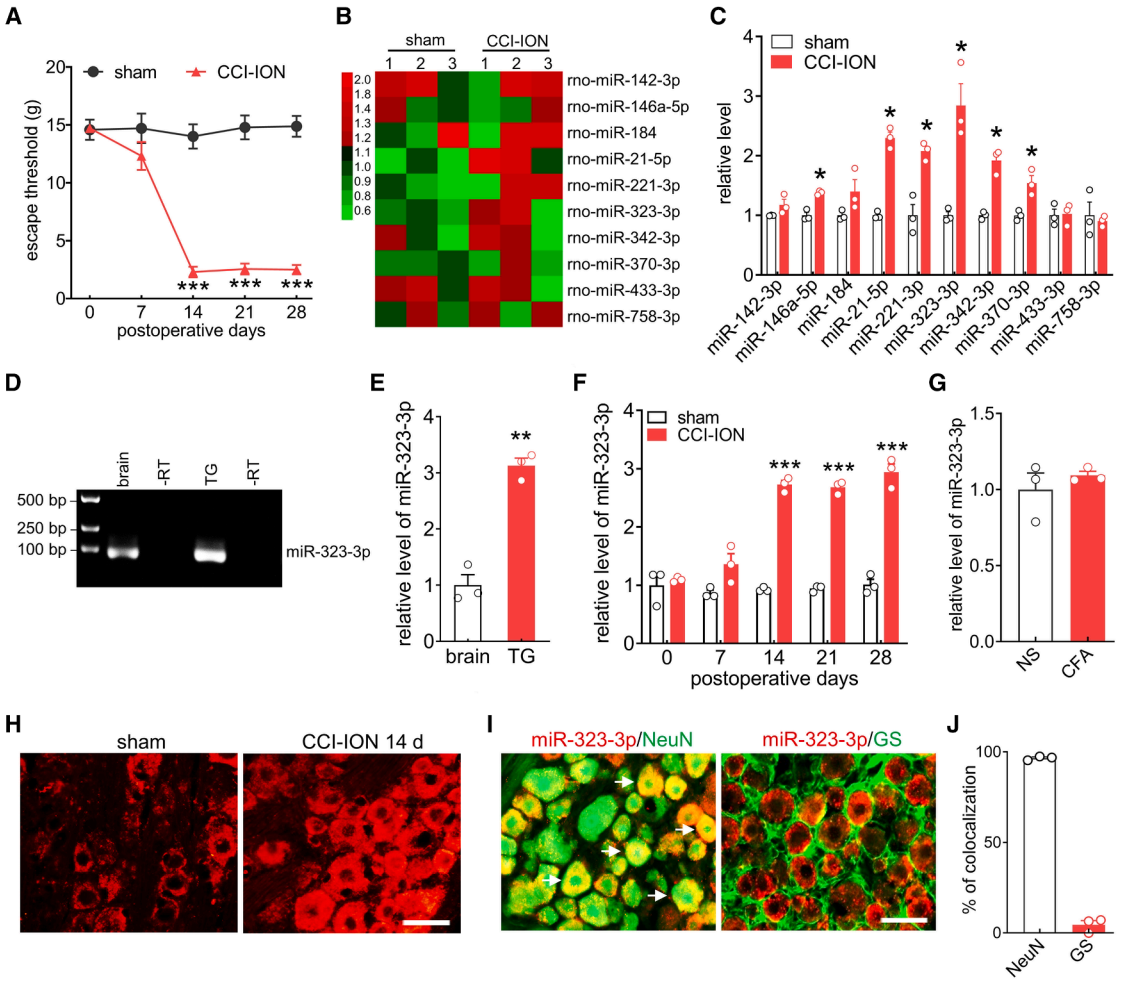

Figure 1. miR-323-3p is upregulated in TG neurons following nerve injury

(A) Escape threshold in the sham- and CCI-ION-operated groups. $n = 6$ rats/group. $^{***}p < 0.001$ (vs. sham) by two-way ANOVA.

(B) Heatmap demonstrated that ten highly conserved miRNAs are significantly upregulated in the injured TGs 14 days after CCI-ION.

(C) Expression levels of ten miRNAs in the ipsilateral TGs 14 days following CCI-ION or sham operation. $n = 3$ rats/group. $^{*}p < 0.05$ (vs. sham) by multiple t test with Holm-Sidak's correction.

(D and E) The expression level of miR-323-3p in the TGs and brain of naive rats. $n = 3$ rats/group. $^{**}p < 0.01$ (vs. brain) by unpaired t test.

(F) Time course of the expression of miR-323-3p in the ipsilateral TGs following CCI-ION or sham surgery. $n = 6$ rats/group. $^{***}p < 0.001$ (vs. sham) by two-way ANOVA.

(G) qPCR analysis of miR-323-3p in the ipsilateral TGs after subcutaneous injection of CFA or normal saline (NS). $n = 3$ rats/group.

(H) RNA FISH of miR-323-3p in the ipsilateral TG 14 days after sham surgery or CCI-ION. Scale bar, 50 μm.

(I) RNA FISH of miR-323-3p, combined with immunofluorescence of NeuN (left) or GS (right). Scale bar, 50 μm.

(J) Bar charts showed the percentage of double-stained TG neurons among total numbers of miR-323-3p^{+}-labeled neurons.

Data are represented as mean ± SEM.

induce miR-323-3p expression specifically in naive TG neurons via transduction of lenti-hSyn-miR-323-3p-up (miR-323-up) (Figure S2B). GFP expression started to be detectable on day 3 and persisted for 21 days (Figure 2G). Similarly, we observed a consistent increase in the expression of miR-323-3p from day 3 through day 21 post-injection of miR-323-up (Figure 2H). The administration of miR-323-up in naive rats led to a significant induction of mechanical hypersensitivity starting on day 3 that persisted for more than 7 days (Figure 2I). In contrast, the same treatment with NC-up did not alter pain behaviors (Figure 2I). Further, we examined whether the regulation of miR-323-3p on CCI-ION-induced mechanical hypersensitivity would be extended to other different neuropathic pain models, including spared nerve injury (SNI) models. As illustrated in Figure 2J, compared to the rats that underwent sham surgery, those that experienced SNI showed a significant decrease ($p < 0.001$) in paw withdrawal threshold (PWT) from day 3 to day 10 after the SNI procedure. When antagomir-323 was intrathecally injected on day 7 after SNI, it significantly alleviated mechanical hypersensitivity from day 1 to day 3 after drug

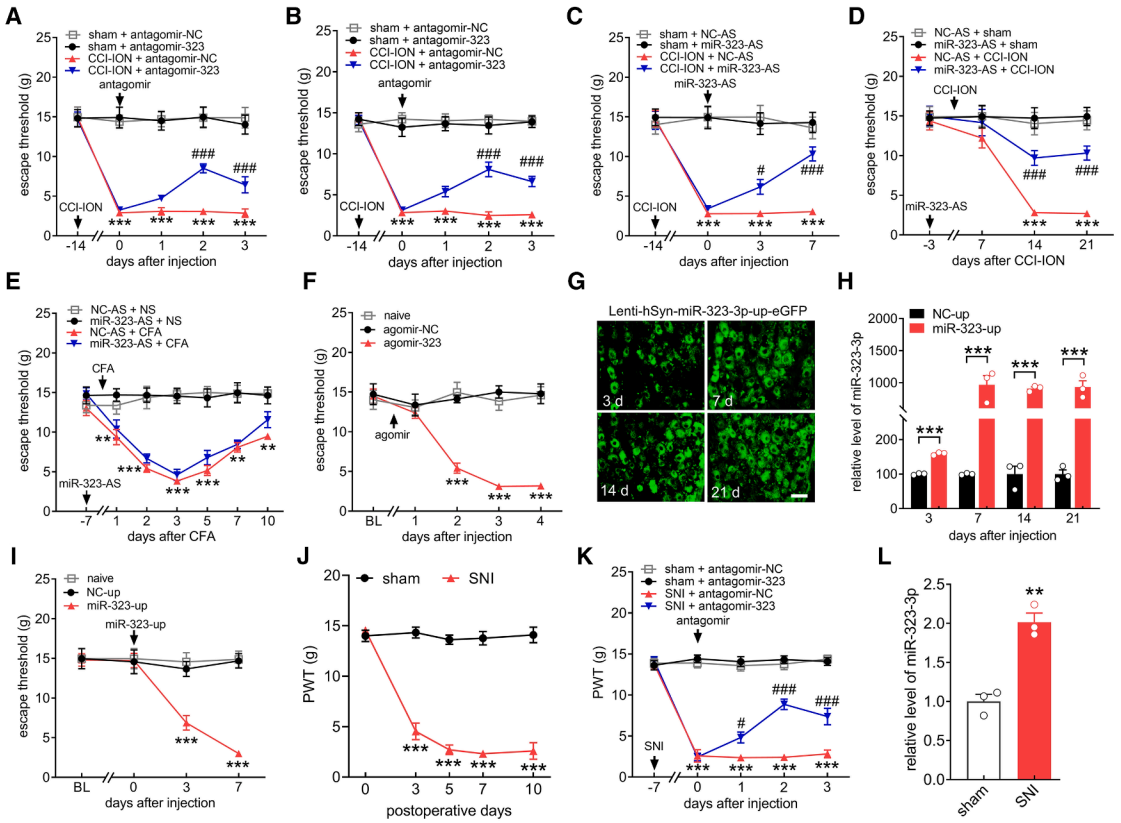

Figure 2. miR-323-3p regulates neuropathic pain behaviors

(A and B) Administration of antagomir-323 alleviated mechanical hypersensitivity 14 days after CCI-ION in male (A) or female (B) rats. $n = 6$ rats/group. $^{***}p < 0.001$ (vs. sham + antagomir-NC) and $^{###}p < 0.001$ (vs. CCI-ION + antagomir-NC) by two-way ANOVA.

(C) Administration of lenti-miR-323-AS alleviated mechanical hypersensitivity 14 days after CCI-ION. $n = 6$ rats/group. $^{***}p < 0.001$ (vs. sham + NC-AS) and $^{#}p < 0.05$ and $^{###}p < 0.001$ (vs. CCI-ION + NC-AS) by two-way ANOVA.

(D) Preadministration of miR-323-AS prevented the nerve-injury-mediated decrease in the escape threshold. $n = 6$ rats/group. $^{***}p < 0.001$ (vs. NC-AS + sham) and $^{###}p < 0.001$ (vs. NC-AS + CCI-ION) by two-way ANOVA.

(E) Administration of miR-323-AS did not affect mechanical hypersensitivity in the CFA-treated rats. $n = 6$ rats/group. $^{**}p < 0.01$ and $^{***}p < 0.001$ (vs. NC-AS + NS) by two-way ANOVA.

(F) Administration of agomir-323 to naive rats enhanced mechanical pain sensitivity. $n = 6$ rats/group. $^{***}p < 0.001$ (vs. agomir-NC) by two-way ANOVA.

(G) Images of EGFP-expressing TG neurons following administration of lenti-hSyn-miR-323-3p-upEGFP (miR-323-up). Scale bar, 50 μm.

(H) qPCR analysis of the expression levels of miR-323-3p following miR-323-up administration. $n = 6$ rats/time point/group. $^{***}p < 0.001$ (vs. NC-up) by two-way ANOVA.

(I) Administration of miR-323-up decreased the escape threshold in naive rats. $n = 6$ rats/group. $^{***}p < 0.001$ (vs. NC-up) by two-way ANOVA.

(J) Paw withdrawal threshold (PWT) in the sham- and SNI-operated groups. $^{***}p < 0.001$ (vs. sham) by two-way ANOVA. $n = 6$ rats/group.

(K) Intrathecal injection of antagomir-323 alleviated mechanical hypersensitivity 7 days after SNI. $^{***}p < 0.001$ (vs. sham + antagomir-NC) and $^{#}p < 0.05$, and $^{###}p < 0.001$ (SNI + antagomir-NC) by two-way ANOVA; $n = 7$ rats/group.

(L) qPCR analysis of miR-323-3p in the ipsilateral DRGs following SNI or sham surgery. $n = 6$ rats/group. $^{**}p < 0.01$ (vs. sham) by unpaired t test.

Data are represented as mean ± SEM.

administration (Figure 2K). Notably, qPCR analysis revealed that the level of miR-323-3p in the injured dorsal root ganglia (DRGs) was remarkably elevated on day 7 in the rats with SNI compared to the sham-operated groups (Figure 2L).

The TF FOXA2 promotes miR-323-3p expression

Gene transcription is tightly regulated by TFs.[17] To identify miR-323-3p regulatory TFs, we performed promoter deletion analysis of the ~2,000 bp 5′ region (bp −2,085 to −13) upstream of *miR-323-3p* and constructed pGL3 luciferase reporter plasmids (labeled pGL3-S1 to pGL3-S5) containing different segments of the *miR-323-3p* promoter (Figure 3A). Measurement of relative luciferase activity showed a dramatic decrease in the group transfected with the pGL3-S2 construct (bp −2,085 to −443) compared with the pGL3-S1 group (Figure 3B), while no significant difference was observed for the other two adjacent fragments. Moreover, both pGL3-S1 and pGL3-ΔS (bp −443 to −13) showed significantly higher luciferase activity than the pGL3 vector ($p < 0.001$), but no difference was observed between these two constructs (Figure 3C). These results indicate

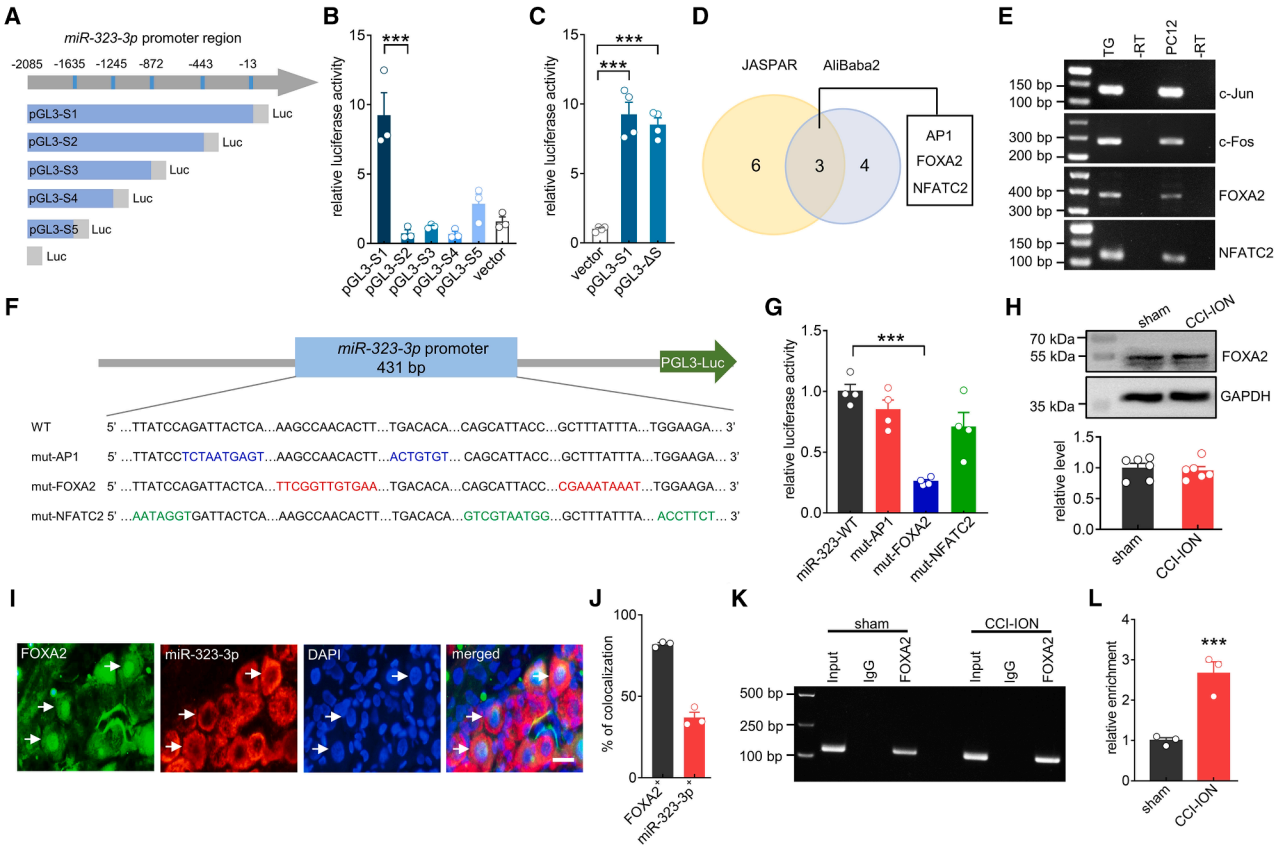

Figure 3. FOXA2 activates miR-323-3p transcription

(A) Schematic diagrams illustrating the pGL3 luciferase reporter constructs that contain different fragments of the *miR-323-3p* promoter (pGL3-S1–S5).

(B) Transcriptional activities of pGL3-S1 to pGL3-S5 measured by luciferase reporter assays. $n = 3$ independent experiments. ***$p < 0.001$ (vs. pGL3-S1) by one-way ANOVA.

(C) Transcriptional activities of pGL3-S1 and pGL3-ΔS. $n = 4$ independent experiments. ***$p < 0.001$ (vs. vector) by one-way ANOVA.

(D) The intersection of AliBaba2 and JASPAR predictions revealed that the ΔS region (−443 to −13 bp) of the *miR-323-3p* promoter contains potential binding sites for AP1, FOXA2, and NFATC2.

(E) RT-PCR analysis of AP1 (Fos/Jun), FOXA2, and NFATC2 in the TGs of naive rats and in PC12 cells.

(F) Schematic diagrams illustrating the plasmids containing the mutant AP1-binding site (mut-AP1), mut-FOXA2, and mut-NFATC2.

(G) Luciferase activity driven by miR-323-WT, mut-AP1, mut-FOXA2, and mut-NFATC2. $n = 4$ independent experiments. ***$p < 0.001$ (vs. miR-323-WT) by one-way ANOVA.

(H) Western blot analysis of FOXA2 expression in the TGs 14 days following sham surgery or CCI-ION. $n = 6$ rats/group.

(I) RNA FISH of miR-323-3p (red) combined with immunofluorescence of FOXA2 (green) and DAPI (blue) in naive TGs. Scale bar, 25 μm.

(J) Statistical analysis showed that ~82.0% of FOXA2-labeled TG cells were positive for miR-323-3p, while ~37.1% of miR-323-3p-labeled TG cells were positive for FOXA2.

(K and L) ChIP-qPCR analysis of FOXA2 binding to the *miR-323-3p* promoter at 14 days following CCI-ION or sham surgery. $n = 6$ rats/group. ***$p < 0.001$ (vs. sham) by unpaired t test.

Data are represented as mean ± SEM.

that the ΔS-containing upstream fragment harbors essential *cis*-regulatory elements controlling *miR-323-3p* expression. We subsequently employed JASPAR (http://jaspar.genereg.net) and AliBaba2.1 (http://gene-regulation.com/pub/programs/alibaba2/) to predict TFs' binding sites within the ΔS promoter region. Three potential factors, namely, activator protein-1 (AP-1) (Fos/Jun), FOXA2, and nuclear factor of activated T cells 2 (NFATC2), were identified (Figure 3D). The expression of these three TFs was confirmed through RT-PCR analysis in both rat TGs and PC12 cells (Figures 3E and S3A). To investigate their functional interactions with the ΔS region, we cloned different luciferase reporter constructs, including mutant (mut)-AP-1, mut-FOXA2, and mut-NFATC2, with mutations in the corresponding TF binding sites (Figure 3F). Interestingly, only mut-FOXA2 showed a significant reduction in luciferase activity compared to that of the wild-type group (miR-323-WT) (Figure 3G). Given the potential role of FOXA2, the expression of FOXA2 protein was examined using immunoblot analysis in TG lysates collected 14 days after CCI-ION. Surprisingly, we did not observe any significant difference in FOXA2 expression

between the CCI-ION- and sham-operated groups (Figures 3H and S3B). ImmunoFISH analysis revealed the coexpression of FOXA2 and miR-323-3p, primarily in the TG neurons of naive rats (Figure 3I). Notably, FOXA2 was predominantly located in the nuclei of TG neurons (stained with DAPI), while miR-323-3p was mainly localized in the cytoplasm (Figure 3I). Statistical analysis indicated that in naive rats, ~81.9% of TG neurons labeled with FOXA2 were positive for miR-323-3p, while ~36.9% of TG neurons labeled with miR-323-3p were positive for FOXA2 (Figure 3J). Based on these findings, we hypothesized that the alteration in miR-323-3p expression driven by CCI-ION might be attributed to changes in FOXA2 binding to the *miR-323-3p* promoter. Chromatin immunoprecipitation (ChIP)-qPCR analysis revealed the amplification of a fragment of the *miR-323-3p* promoter containing the binding motif from the immunoprecipitate obtained with the anti-FOXA2 antibody (Figures 3K and S3C). Compared to that of the sham surgery, the occupancy of FOXA2 on the *miR-323-3p* promoter was significantly enhanced on day 14 following CCI-ION (Figure 3L).

PRMT2-mediated H3R8me2a increases the binding of FOXA2 to miR-323-3p

DNA methylation and histone modifications are key epigenetic mechanisms regulating gene expression by modulating TF binding.[18] Using MethPrimer (www.urogene.org/methprimer/), we detected no CpG islands in the *miR-323-3p* promoter region (Figure S4), ruling out the possibility of DNA methylation in miR-323-3p regulation. Emerging evidence suggests that histone modifications, particularly protein arginine methylation, are implicated in regulating fundamental cellular processes, including gene transcription and RNA processing.[19–21] We thus evaluated the activity of PRMTs after trigeminal nerve injury. Analysis of our RNA-seq dataset (Database: GSE224814) revealed that among all detectable PRMT family members (PRMT1–5 and PRMT7–9), only PRMT2 was significantly upregulated, with a 1.37-fold increase in the injured TGs after CCI-ION (Figure 4A). Further immunoblot analysis revealed that the protein expression of PRMT2 was also increased at 14 days following CCI-ION operation compared to sham surgery (Figures 4B and S5A). PRMT2 is responsible for the maintenance of H3R8me2a, and PRMT2-dependent H3R8me2a is needed for transcriptional regulation of its target genes.[22] Thus, we assessed the methylated H3R8 histone form and found that the H3R8me2a protein level in the TGs was significantly increased 14 days after CCI-ION compared with sham surgery (Figures S5B and S5C). In the subsequent immunoFISH analysis, H3R8me2a was predominantly localized within the nuclei of TG neurons (as indicated by DAPI staining) and was coexpressed with miR-323-3p in both the CCI-ION and sham groups (Figure 4C). Most neurons with higher levels of H3R8me2a also showed high expression of miR-323-3p in the rats subjected to CCI-ION operation (Figure 4C). Quantitative analysis showed that ~44.7% of DAPI-labeled TG cells were both miR-323-3p-positive and H3R8me2a-positive in sham surgery, while ~75.1% were in CCI-ION operation (Figure 4D). Moreover, ChIP-PCR assays revealed the amplification of a *miR-323-3p* promoter fragment in the anti-H3R8me2a complexes compared to the immunoglobulin (Ig)G control complexes (Figures 4E and S5D). On day 14 post-CCI-ION, the *miR-323-3p* promoter exhibited significantly higher H3R8me2a occupancy than that observed after sham surgery (Figure 4E). Additionally, we further investigated whether the PRMT2-mediated regulation of H3R8me2a plays a functional role in the development of nerve-injury-induced mechanical hypersensitivity. To achieve this, we used a chemically modified small interfering RNA (PRMT2-siRNA) to specifically knock down the expression of PRMT2. Intra-TG injection of PRMT2-siRNA in the injured TGs abrogated the increase in the protein expression of PRMT2 induced by CCI-ION (Figures S5E and S5F). ChIP-qPCR analysis of TG lysates showed that the administration of PRMT2-siRNA significantly decreased the amplification of the *miR-323-3p* promoter fragment from the anti-H3R8me2a complex (Figures 4F and S5G) and the anti-FOXA2 complex (Figures 4G and S5H) in the injured TGs following CCI-ION. Moreover, intra-TG injection of PRMT2-siRNA in the injured TGs abrogated the upregulation of miR-323-3p expression induced by CCI-ION (Figure 4H). Furthermore, the administration of PRMT2-siRNA, but not NC-siRNA, attenuated nerve-injury-induced mechanical hypersensitivity on day 14 after surgery (Figure 4I).

miR-323-3p targets Kv2.1 potassium channels

miRNAs regulate gene expression by binding to the 3′ UTRs of their target mRNAs, thereby inhibiting their use by either degradation or translational repression.[23] To identify miR-323-3p target genes potentially involved in neuropathic pain, we cross-referenced predictions from TargetScan (http://www.targetscan.org) and miRWalk (http://mirwalk.umm.uni-heidelberg.de/) databases, identifying 21 candidate genes through overlapping results (Figure 5A). Searching for these 21 candidates in our RNA-seq database (Database: GSE224814) revealed that five genes, namely, gremlin 2 (*GREM2*),[24] potassium voltage-gated channel subfamily B member 1 (*KCNB1*),[25] visinin-like 1 (*VSNL1*),[26] ATPase phospholipid transporting 11A (*ATP11A*),[27] and fragile X messenger ribonucleoprotein 1 (*FMR1*),[28] were significantly downregulated in injured TGs of the rats subjected to CCI-ION, and their expression was then confirmed by qPCR (Figure 5B). We focused mainly on KCNB1, a Kv2.1 channel-encoding gene, because qPCR analysis revealed that the KCNB1 mRNA level exhibited the greatest decrease (>50%) in the injured TGs (Figure 5B), and Kv2.1 has been shown to play critical roles in controlling sensory neuron excitability.[25,29] To investigate whether miR-323-3p directly targets Kv2.1, we constructed luciferase reporter plasmids by inserting the 3′ UTR of KCNB1, which contains the WT (Kv2.1-wt) or mutant miR-323-3p target sequence (Kv2.1-mut), downstream of the firefly luciferase gene (Figure 5C). Compared with that of the NC mimic, the luciferase activity of the Kv2.1-wt reporter was markedly reduced in the cells cotransfected with the miR-323-3p mimic, and this inhibition was reversed by transfection of the Kv2.1-mut reporter plasmid (Figure 5D). The miR-323-3p-binding sites that were predicted by the TargetScan database (http://www.targetscan.org) exhibit a high degree of conservation across vertebrates (Figure 5E), demonstrating that these binding sites have functional importance in the regulation of Kv2.1. Furthermore, we investigated whether the modulation of miR-323-3p expression alters the function of Kv2.1 channels. ImmunoFISH revealed that miR-323-3p colocalized with Kv2.1 in

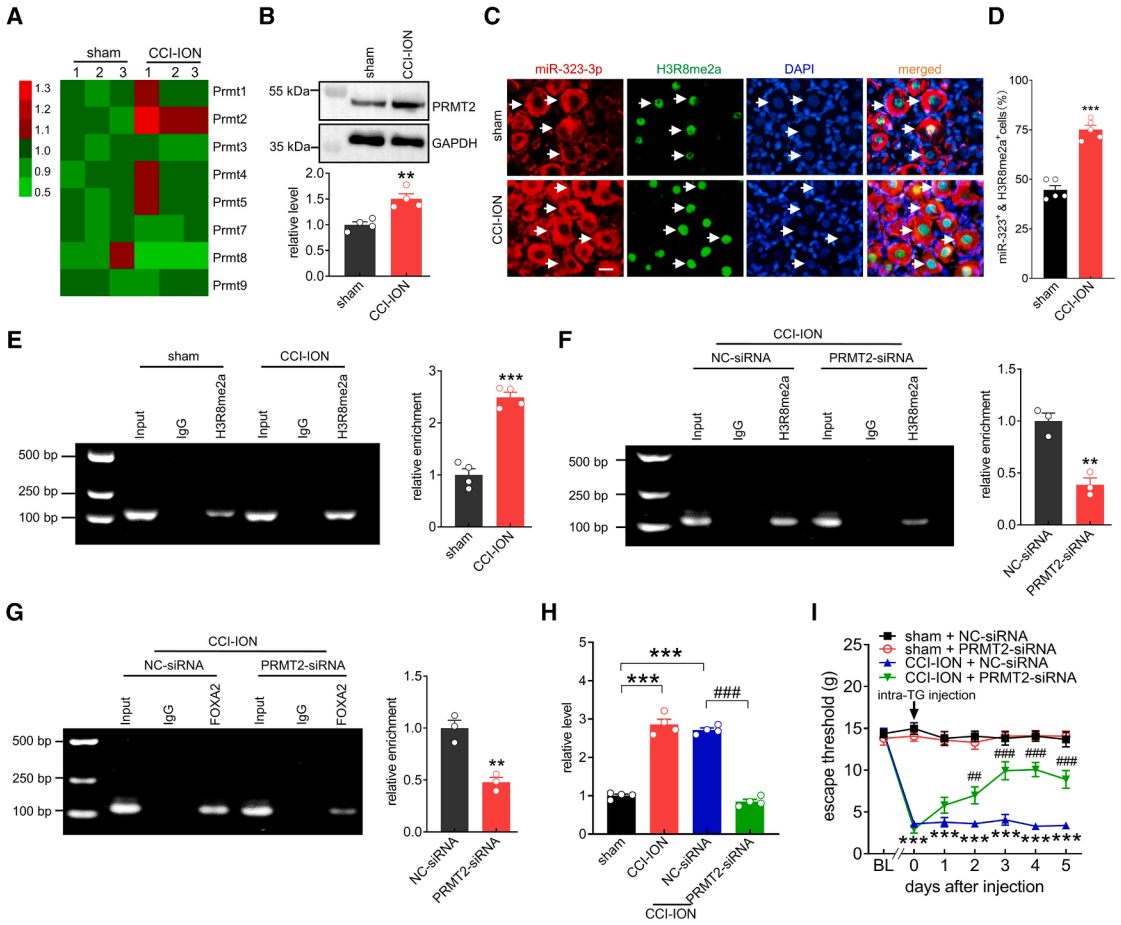

Figure 4. PRMT2-mediated H3R8me2a increases FOXA2 binding to miR-323-3p

(A) Heatmap of RNA sequencing data indicating the expression of 8 PRMT family genes (PRMT1–5 and PRMT7–9) in the ipsilateral TGs 14 days following CCI-ION or sham operation.

(B) Representative immunoblots (top) and summary data (bottom) indicating the expression of PRMT2 in the injured TGs at 14 days following CCI-ION or sham surgery. $n = 8$ rats/group. $^{**}p < 0.01$ (vs. sham) by unpaired t test.

(C) RNA FISH of miR-323-3p (red) combined with immunofluorescence of H3R8me2a (green) and DAPI (blue) in TGs 14 days after CCI-ION or sham surgery. Scale bar, 25 μm.

(D) Bar charts showed the percentage of both miR-323-3p^{+} and H3R8me2a^{+} TG neurons among total numbers of DAPI-labeled TG cells. $n = 5$ rats/group. $^{***}p < 0.001$ (vs. sham) by unpaired t test.

(E) ChIP-qPCR analysis of H3R8me2a binding to the promoter region of *miR-323-3p* at 14 days after CCI-ION or sham surgery. $n = 8$ rats/group. $^{***}p < 0.001$ (vs. sham) by unpaired t test.

(F) Administration of PRMT2-siRNA prevented the increase in the level of H3R8me2a in the injured TGs of the rats subjected to CCI-ION. $n = 6$ rats/group. $^{**}p < 0.01$ (vs. CCI-ION + NC-siRNA) by unpaired t test.

(G) Administration of PRMT2-siRNA suppressed FOXA2 binding to the *miR-323-3p* promoter 14 days following CCI-ION. $n = 6$ rats/group. $^{**}p < 0.01$ (vs. CCI-ION + NC-siRNA) by unpaired t test.

(H) Administration of PRMT2-siRNA prevented the increase in the expression of miR-323-3p in the injured TGs of the rats subjected to CCI-ION. $n = 8$ rats/group. $^{***}p < 0.001$ (vs. sham) and $^{###}p < 0.001$ (vs. CCI-ION + NC-siRNA) by one-way ANOVA.

(I) Administration of PRMT2-siRNA attenuated mechanical hypersensitivity on day 14 following CCI-ION operation. $n = 7$ rats/group. $^{***}p < 0.001$ (vs. sham + NC-siRNA) and $^{##}p < 0.01$ and $^{###}p < 0.001$ (vs. CCI-ION + NC-siRNA) by two-way ANOVA.

Data are represented as mean ± SEM.

TG neurons after sham surgery (Figure 5F). Compared to the rats with sham surgery, the CCI-ION-treated rats showed a higher miR-323-3p expression level but a comparatively lower Kv2.1 protein expression level 14 days after surgery (Figures 5F and 5G). The Kv2.1 mRNA level was decreased in the injured TGs 14, 21, and 28 days after CCI-ION, while no significant changes were observed after sham surgery (Figure 5H). The decreased expression of Kv2.1 mRNA was inversely correlated with the upregulation of miR-323-3p (Figure 5I). Moreover, the administration of agomir-323, but not agomir-NC, caused a dramatic reduction in the expression of Kv2.1 channel proteins in naive TGs (Figures 5J and S6A). Moreover, whole-cell patch-clamp recordings of

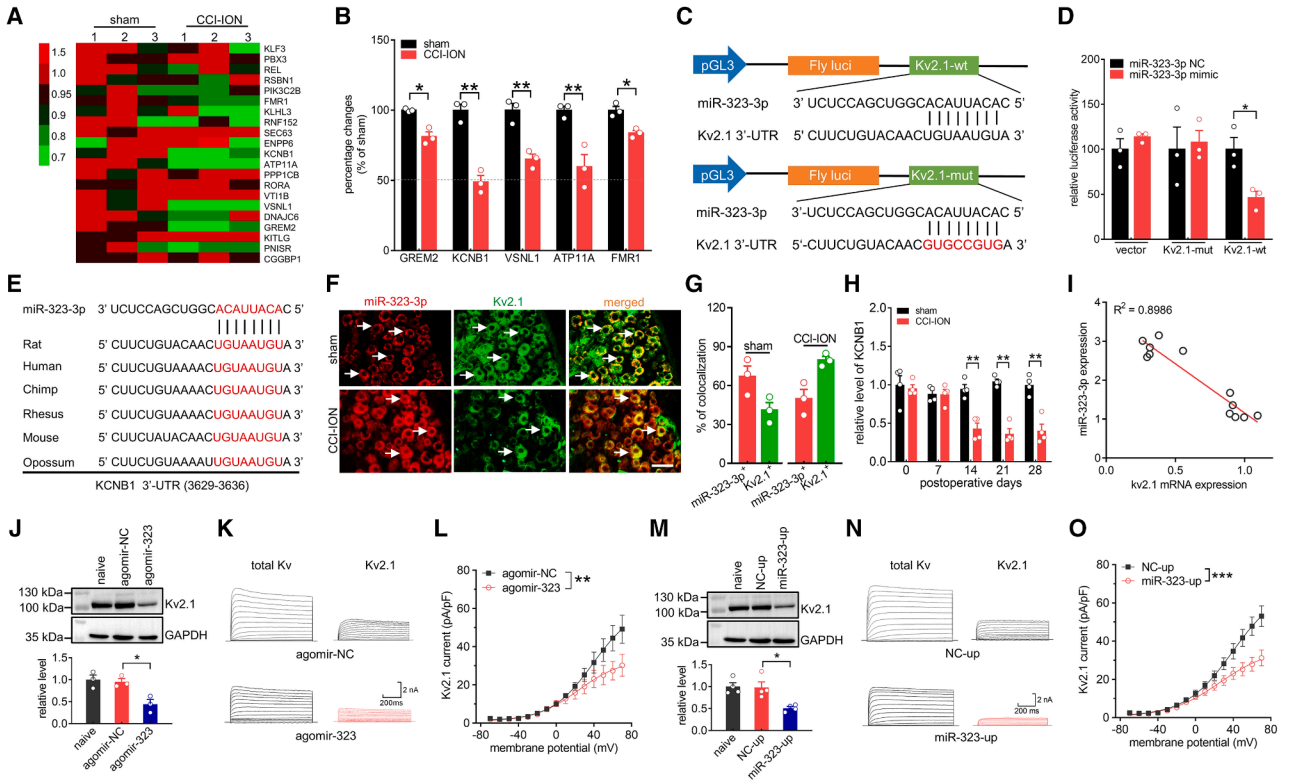

Figure 5. miR-323-3p targets Kv2.1 potassium channels

(A) Heatmap showing expression of predicted miR-323-3p target genes (TargetScan/miRWalk) in TGs 14 days post-CCI-ION or sham surgery.

(B) Five of the predicted target genes were downregulated in the injured TGs 14 days following CCI-ION. $n = 3$ rats/group. $^{*}p < 0.05$ and $^{**}p < 0.01$ (vs. sham) by multiple t test with Holm-Sidak's correction.

(C) Schematic diagrams illustrating luciferase reporter constructs containing either wild-type Kv2.1 (Kv2.1-wt) or mutant Kv2.1 (Kv2.1-mut).

(D) Relative luciferase activity in Kv2.1-wt and Kv2.1-mut cells after transfection with the miR-323-3p mimic or its negative control (NC). $n = 3$ rats/group. $^{*}p < 0.05$ (vs. miR-323-3p NC + Kv2.1-wt) by multiple t test with Holm-Sidak's correction.

(E) Diagrams displaying the sequences of Kv2.1. 3′ UTRs from various vertebrates with a high conservation of miR-323-3p-binding sites.

(F) RNA FISH of miR-323-3p (red) combined with immunofluorescence of Kv2.1 (green) in the sham- and CCI-ION-operated groups. Scale bar, 50 μm.

(G) Percentage of double-labeled TG neurons among total miR-323-3p- or Kv2.1-positive neurons.

(H) Kv2.1 mRNA expression in the sham- and CCI-ION-operated groups. $n = 8$ rats/group. $^{**}p < 0.01$ (vs. sham) by two-way ANOVA.

(I) Linear regression analysis of the expression level of miR-323-3p vs. that of Kv2.1 mRNA in the injured TGs.

(J) Intra-TG injection of agomir-323 decreased Kv2.1 protein expression in the TGs of naive rats. $n = 6$ rats/group. $^{*}p < 0.05$ (vs. agomir-NC) by one-way ANOVA.

(K and L) Representative traces (K) and bar graph (L) indicating Kv2.1 channel currents recorded in the agomir-323- and agomir-NC-treated TG neurons. $n = 15$–17 neurons/group. $^{**}p < 0.01$ (vs. agomir-NC) by two-way ANOVA.

(M) Administration of miR-323-up decreased the protein expression of Kv2.1 in the TGs of naive rats. $n = 8$ rats/group. $^{*}p < 0.05$ (vs. NC-up) by one-way ANOVA.

(N and O) Representative traces (N) and bar graph (O) indicating Kv2.1 channel currents recorded in the miR-323-up- and NC-up-transduced TG neurons. $n = 15$–16 neurons/group. $^{***}p < 0.001$ (vs. NC-up) by two-way ANOVA.

Data are represented as mean ± SEM.

small-sized TG neurons retrogradely labeled with DiI revealed that administration of agomir-323 markedly decreased Kv2.1 channel currents (Figures 5K and 5L). In support of these findings, further local induction of miR-323-3p expression in the TG neurons of naive rats robustly reduced Kv2.1 protein expression (Figures 5M and S6B) and suppressed Kv2.1 channel currents (Figures 5N and 5O).

Kv2.1 channels participate in regulating neuropathic pain behaviors

Next, we investigated whether Kv2.1 channels participate in regulating trigeminal-mediated neuropathic pain behaviors. At 14, 21, and 28 days following CCI-ION operation, the protein abundance of Kv2.1 was markedly decreased (Figures 6A and S7A). The sham operation did not induce any significant alterations in the protein abundance of Kv2.1 in the ipsilateral TGs (Figures 6B and S7B). In addition, Kv2.1 protein expression in the contralateral TGs remained unaltered following CCI-ION throughout the experimental period (Figures S7C and S7D). Immunostaining analysis indicated that Kv2.1 was colocalized with NeuN but was not detected in GS-labeled cells, indicating that Kv2.1 is expressed predominantly in TG neurons. Quantitative analysis revealed that ~91.1% of $Kv2.1^{+}$ cells were $NeuN^{+}$ and only ~2.7% were GS^{+} (Figure 6C). Further quantitative data showed

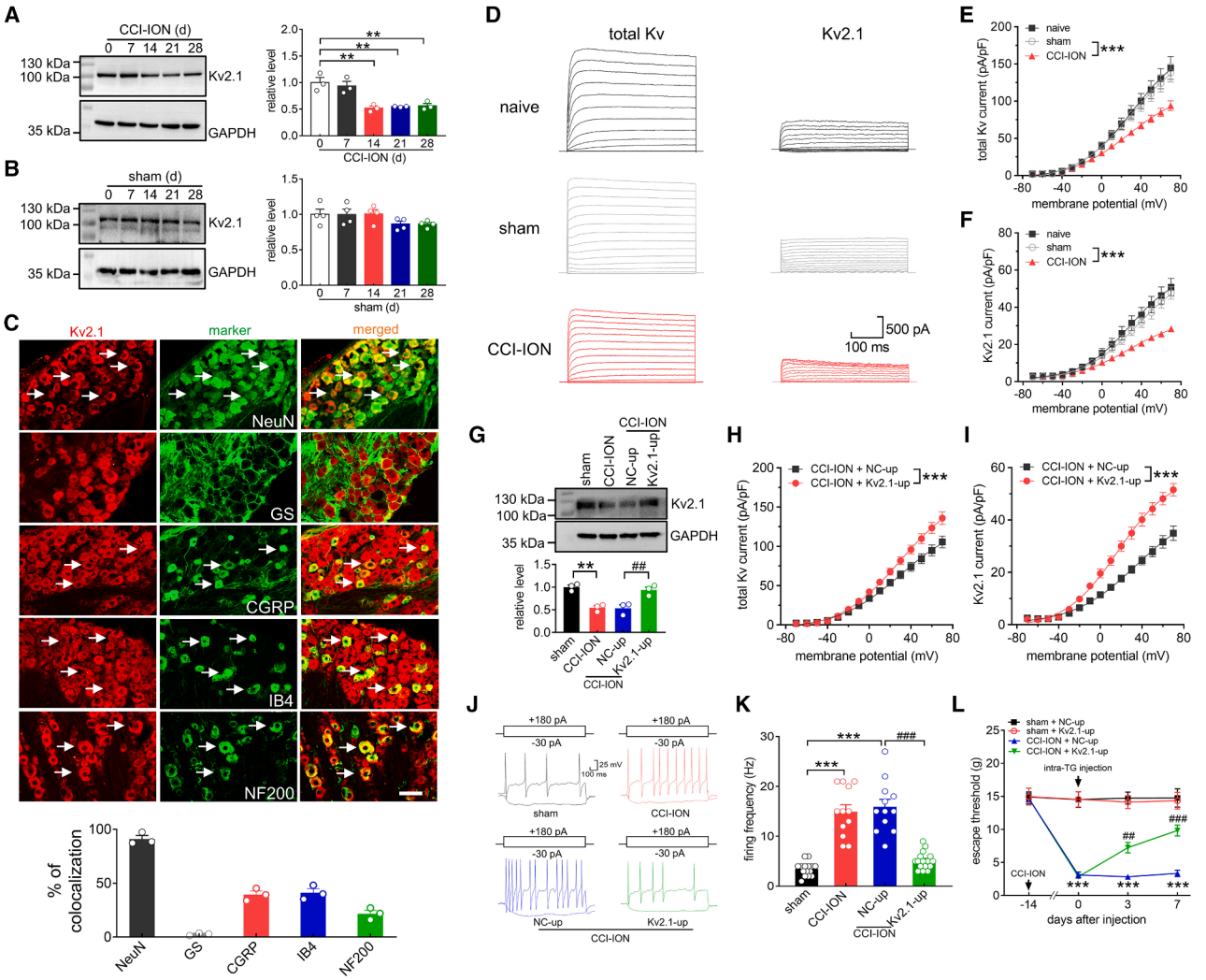

Figure 6. Kv2.1 channels participate in regulating neuropathic pain behaviors

(A and B) Time course of the protein abundance of Kv2.1 in TGs following CCI-ION (A, $n = 6$ rats/group) or sham operation (B, $n = 8$ rats/group). $^{**}p < 0.01$ (vs. Kv2.1, day 0) by one-way ANOVA.

(C) Double immunostaining of Kv2.1 (red) with NeuN, GS, IB_4, CGPR, or NF200 (green) in naive TGs. Bar charts show the percentage of double-stained TG neurons among total numbers of $Kv2.1^+$-labeled cells. $n = 3$ rats/group. Scale bar, 50 μm.

(D) Representative traces of the total Kv and Kv2.1 channel currents recorded in small TG neurons 14 days following CCI-ION or sham operation.

(E and F) Summary data showing the total Kv (E) and Kv2.1 (F) channel currents indicated in (D). $n = 11$–12 neurons/group. $^{***}p < 0.001$ (vs. sham) by two-way ANOVA.

(G–I) Administration of lenti-hSyn-Kv2.1-up (Kv2.1-up) suppressed the nerve-injury-induced reduction in Kv2.1 protein abundance (G, $n = 6$ rats/group), the total Kv current (H, $n = 15$ neurons/group), and the Kv2.1 channel current (I, $n = 15$ neurons/group). (G) $^{**}p < 0.01$ (vs. sham) and $^{\#\#}p < 0.01$ (vs. CCI-ION + NC-up) by one-way ANOVA. (H and I) $^{***}p < 0.001$ (vs. CCI-ION + NC-up) by two-way ANOVA.

(J and K) Representative traces (J) and summary data (K) indicating that intra-TG administration of Kv2.1-up prevented the CCI-ION-induced increase in the action potential firing rate. $n = 12$–16 neurons/group. $^{***}p < 0.001$ (vs. sham) and $^{\#\#\#}p < 0.001$ (vs. CCI-ION + NC-up) by one-way ANOVA.

(L) Intra-TG injection of Kv2.1-up alleviated CCI-ION-induced mechanical hypersensitivity. $n = 6$ rats/group. $^{***}p < 0.001$ (vs. sham + NC-up) and $^{\#\#}p < 0.01$ and $^{\#\#\#}p < 0.001$ (vs. CCI-ION + NC-up) by two-way ANOVA.

Data are represented as mean ± SEM.

that ~39.4% of $Kv2.1^+$ neurons were $CGRP^+$, ~41.1% were IB_4^+, and ~21.7% were 200 kD neurofilament protein (NF200)-positive ($NF200^+$) (Figure 6C). Next, we examined whether the CCI-ION-induced decrease in Kv2.1 protein abundance affects Kv2.1 channel currents. Recording of DiI-labeled small neurons revealed that CCI-ION, but not sham surgery, markedly decreased both the total Kv (Figures 6D and 6E) and Kv2.1 (Figures 6D and 6F) channel currents. Local induction of Kv2.1 expression in TG neurons of naive rats utilizing a lentiviral vector containing a neuron-specific promoter, lenti-hSyn-Kv2.1-up (Kv2.1-up),

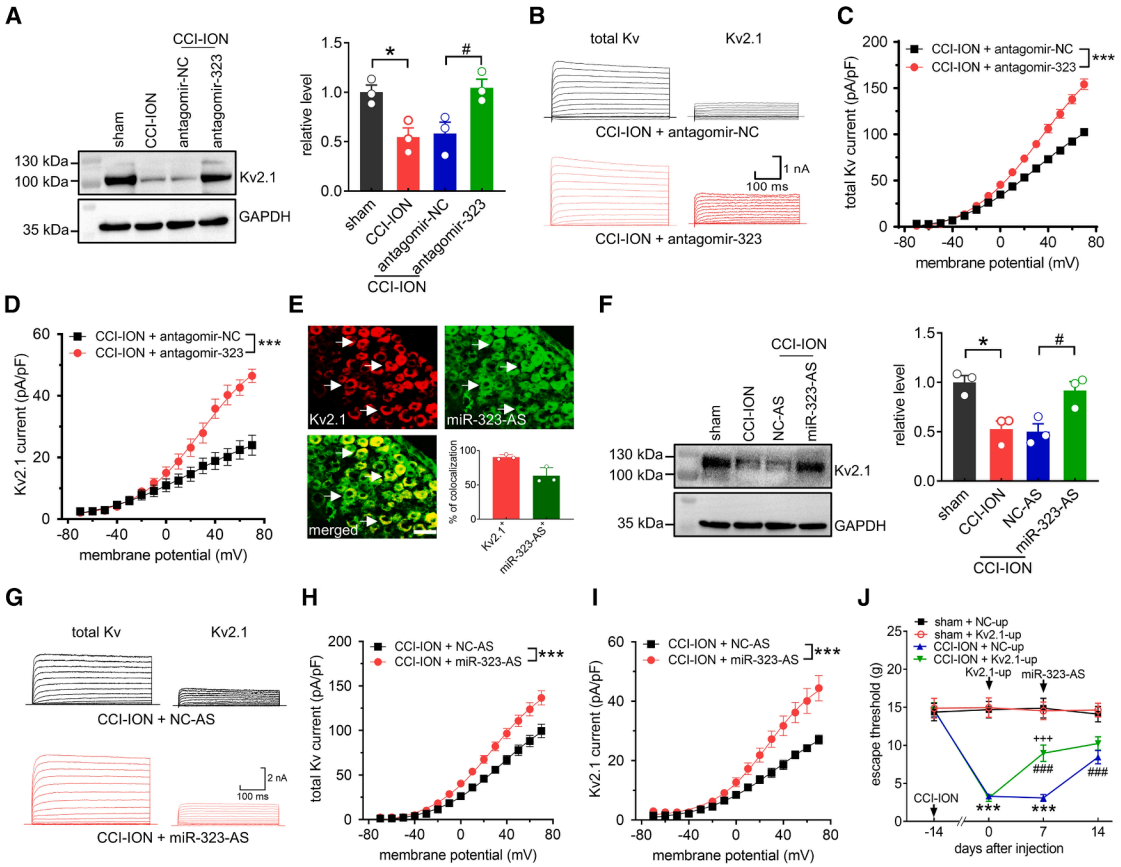

Figure 7. miR-323-3p regulates nociceptive behaviors via Kv2.1 channels

(A) Administration of antagomir-323, but not antagomir-NC, reversed the nerve-injury-induced decrease in Kv2.1 protein abundance. $n = 3$ rats/group. $^{*}p < 0.05$ (vs. sham) and $^{\#}p < 0.05$ (vs. CCI-ION + antagomir-NC group) by one-way ANOVA.

(B–D) Example traces (B) and summary data indicating the total Kv (C) and Kv2.1 (D) channel currents in small TG neurons of the rats subjected to CCI-ION on day 3 after antagomir-323 or antagomir-NC administration. $n = 11$–12 neurons/group. $^{***}p < 0.05$ (vs. CCI-ION + antagomir-NC) by two-way ANOVA.

(E) RNA FISH of miR-323-3p (red) combined with immunofluorescence of Kv2.1 (green) in the TGs at 7 days after miR-323-AS administration. Scale bar, 50 μm. Inset, bar graph indicating the percentages of double-stained TG neurons among miR-323-AS-transduced neurons and Kv2.1-positive neurons.

(F) Injection of miR-323-AS reversed the nerve-injury-induced reduction in Kv2.1 protein abundance. $n = 6$ rats/group. $^{*}p < 0.05$ (vs. sham) and $^{\#}p < 0.05$ (vs. CCI-ION + NC-AS) by one-way ANOVA.

(G–I) Example traces (G) and summary of results showing the total Kv (H) and Kv2.1 (I) channel currents in small TG neurons of the rats subjected to CCI-ION on day 7 after administration of miR-323-AS or NC-AS. $n = 14$–15 neurons/group. $^{***}p < 0.05$ (vs. CCI-ION + NC-AS) by two-way ANOVA.

(J) Effects of Kv2.1-up (day 0) and NC-up (day 7) on miR-323-AS-induced alleviation of mechanical hypersensitivity in the rats subjected to CCI-ION. $n = 6$ rats/group. $^{***}p < 0.001$ (vs. sham + NC-up), $^{\#\#\#}p < 0.001$ (vs. CCI-ION + NC-up, Day 7), and $^{+++}p < 0.001$ (vs. CCI-ION + Kv2.1, day 0) by two-way ANOVA.

Data are represented as mean ± SEM.

significantly increased the protein abundance of Kv2.1 (Figures 6G and S7E) and induced consistent increases in the total Kv and Kv2.1 channel currents on day 7 post-injection, but these effects were not observed after transduction of NC-up (Figures 6H and 6I). In addition, intra-TG injection of Kv2.1-up abrogated the increase in the action potential firing rate induced by CCI-ION (Figures 6J and 6K). Moreover, the administration of Kv2.1-up markedly alleviated mechanical hypersensitivity induced by CCI-ION from day 3 to day 7 (Figure 6L).

miR-323-3p regulates nociceptive behaviors via Kv2.1 channels

We examined whether miR-323-3p modulation alters Kv2.1 protein expression in the injured TGs. Intra-TG administration of antagomir-323, but not antagomir-NC, dramatically reversed the decrease in Kv2.1 expression 14 days after CCI-ION (Figures 7A and S8A). Recording of DiI-labeled small neurons showed that the administration of antagomir-323 significantly reversed the nerve-injury-induced decrease in both the total Kv (Figures 7B and 7C) and Kv2.1 (Figures 7B and 7D) channel currents. To further corroborate these findings, we employed a knockdown strategy to decrease the expression of miR-323-3p in the TGs by injection of miR-323-AS. We observed the expression of EGFP-labeled miR-323-3p after miR-323-AS transduction in neurons of various sizes (Figure 7E). Statistical analysis revealed that approximately 89.5% of $Kv2.1^{+}$ neurons expressed miR-323-AS and that 60.3% of miR-323-AS^{+} neurons expressed Kv2.1 (Figure 7E). Immunoblot analysis showed that

administration of miR-323-AS reversed the nerve-injury-induced reduction in Kv2.1 protein abundance (Figures 7F and S8B). Similarly, recordings of DiI-labeled small neurons indicated that blockade of miR-323-3p significantly reversed the CCI-ION-mediated decrease in both the total Kv (Figures 7G and 7H) and Kv2.1 (Figures 7G and 7I) channel currents. To gain further insights into the role of Kv2.1 as a mediator of miR-323-3p-induced nociceptive behaviors, we conducted local delivery of Kv2.1-up and miR-323-AS into the injured TGs after CCI-ION. Kv2.1-up was intra-TG administered on day 0, followed by the administration of miR-323-AS on day 7. As shown in Figure 7J, the Kv2.1-up treatment, compared to the NC (NC-up), significantly alleviated CCI-ION-induced mechanical hypersensitivity (Figure 7J). Additionally, the administration of miR-323-AS on day 7 did not demonstrate any additional effect on the mechanical threshold in the rats that underwent CCI-ION and received Kv2.1-up treatment. This finding was evident from the stable mechanical threshold observed from day 7 to day 14 subsequent to the administration of miR-323-AS (Figure 7J). In contrast, the rats subjected to CCI-ION and treated with NC-up or intra-TG injection of miR-323-AS showed a significantly increased mechanical pain threshold (Figure 7J).

DISCUSSION

In the present study, we identified a PRMT2/FOXA2/miR-323-3p/Kv2.1 signaling axis in sensory neurons that contributes to trigeminal neuropathic pain. miR-323-3p upregulation is causally involved in the development of neuropathic pain, and inhibition of miR-323-3p (pharmacologically or genetically) alleviates nociceptive behaviors. Mechanistically, nerve injury induces the upregulation of PRMT2, which promotes H3R8me2a, thereby facilitating the binding of the TF FOXA2 to the promoter of *miR-323-3p*, leading to the upregulation of *miR-323-3p* expression. Moreover, miR-323-3p targets Kv2.1, in turn affecting TG neuron excitability and eventually leading to neuropathic pain symptoms (see Figure S9). Modulation of epigenetic factors in the PRMT2/FOXA2/miR-323-3p/Kv2.1 signaling pathway may advance the discovery of therapeutic strategies for neuropathic pain.

miRNAs play important roles in the post-transcriptional regulation of gene expression by binding to specific complementary sequences in target mRNAs.[8,30] Increasing evidence has suggested that miRNA expression can undergo tissue-/cell-type-specific changes in response to different pain conditions and that the modulation of miRNA expression prevents and reverses persistent inflammatory, neuropathic, and cancer-related nociceptive behaviors.[31–34] However, the regulation of miRNAs by epigenetic mechanisms and their interplay in neuropathic pain are not fully understood. Modifications of histones and DNA methylation are the two main epigenetic regulatory mechanisms that have profound effects on gene expression.[35,36] Previous studies have indicated that DNA methylation and hydroxylation regulate miRNA expression in the context of inflammatory pain.[33,37] Here, examination of the miR-323-3p gene sequence excluded this possibility, as no CpG island was found within the *miR-323-3p* promoter. Instead, we revealed that nerve injury significantly increased the expression of PRMT2, promoting H3R8 dimethylation in the *miR-323-3p* promoter, and showed that these modifications mediated by PRTM2 upregulation in the TGs led to increased pain sensitivity. PRMT2 is the key PRMT involved in many cellular processes, including gene transcription and RNA processing.[38] Although little is known regarding the role of PRMT2 in pain regulation, emerging evidence from RNA-seq analysis has identified potential roles for PRMT2 in nociceptive behaviors. Consistent with the results of our present study, previous research by Xu and co-workers demonstrated that the expression of PRMT2 in the DRG was upregulated after spinal nerve ligation (SNL).[39] Interestingly, contradictory results in another study revealed a significant reduction in PRMT2 expression in the DRG in a rat model of complex regional pain syndrome type 1.[40] However, in mouse models of inflammatory temporomandibular joint pain, the transcript levels of both PRMT1 and PRMT2 in the spinal trigeminal nucleus caudalis presented no significant changes following injury,[41] while in another study, nerve injury induced a reduction in PRMT1 expression in the anterior cingulate cortex (ACC).[42] Here, in rat TG neurons, we demonstrated that PRMT2, but not other PRMT family members, was selectively upregulated in injured TGs after nerve injury. One possible explanation for these discrepancies is the differences in the transcriptomic and epigenomic profiles between the central nervous system (CNS) and the peripheral nervous system (PNS). These inherent differences in gene expression and regulation could contribute to the observed variations between the CNS and PNS. Indeed, it has been demonstrated that SNI causes differential gene expression in the central spinal dorsal horn and DRG in rats.[43] More interestingly, studies have shown that even within the same tissue, different pain models induce significant differences in gene expression profiles.[44] Thus, the diversity of target genes regulated by PRMT2 in the CNS and/or PNS may increase the complexity of its regulatory role in pain processing. Furthermore, the detectable expression of PRMT2 and its anti-inflammatory effects has been demonstrated in non-neuronal cells, including microglia and glioblastoma cells.[22,45] Further investigation is required to elucidate the role of PRMT2-mediated anti-inflammation in trigeminal-mediated neuropathic pain; however, we consider this to be outside the scope of the present study.

Voltage-gated K^+ channels (Kv) play critical roles in regulating neuronal excitability, which is responsible for nociceptive signal processing.[46] Indeed, peripheral nerve-injury-induced dysfunction of Kv channels induces a reduction in the associated currents, triggering sensory neuron hyperexcitability and resulting in pain hypersensitivity.[25,47] Opening of Kv channels or restoration of Kv currents leads to the restriction of neuronal excitability and induces antinociception.[48] The Kv2.1 channel, encoded by KCNB1, is the main contributor to neuronal delayed rectifying potassium currents responsible for AP repolarization.[49] Unlike the predominant expression of Kv2.1 in the small IB_4-binding and CGRP populations in peripheral TG neurons, previous studies using *in situ* hybridization analysis of rat DRG have shown that KCNB1 mRNA expression is abundant in cells of all sizes, being particularly plentiful in the large NF200 population.[50,51] While TGs and DRGs both house peripheral sensory neurons with overlapping functions, they arise from distinct developmental lineages and exhibit notable molecular differences, as highlighted by recent high-resolution transcriptomic

studies.[51] These intrinsic differences may account for the observed divergence in KCNB1/Kv2.1 expression patterns. Notably, pre-adsorption of the Kv2.1 antibody with its blocking peptide eliminated Kv2.1 immunofluorescence in TGs, confirming antibody specificity (Figure S10). Previous studies have shown that Kv2.1 currents are reduced in the injured DRG following traumatic nerve injury, resulting in pain hypersensitivity.[50] Moreover, the administration of nerve growth factor was shown to restore the Kv2.1 current and provide neuroprotective effects after nerve transection.[52] However, the functional role of Kv2.1 in trigeminal-mediated nociceptive processing remains unclear. Our findings showed that peripheral nerve injury triggers the downregulation of Kv2.1 expression and that local induction of Kv2.1 channel expression in TG neurons alleviates CCI-ION-induced mechanical hypersensitivity. Consistent with our current findings, knocking down Kv2.1 channels in the DRG induced hyperexcitability of peripheral nociceptors and promoted nociception.[25]

Taken together, the results of our current study provide insights into a PRMT2/FOXA2/miR-323-3p/Kv2.1 signaling axis in sensory neurons that participates in the pathogenesis of trigeminal neuropathic pain. The identification of epigenetic modifiers, including PRMT2, FOXA2, and miR-323-3p, in regulating sensory neuronal Kv2.1 channels may provide insight into possibilities for developing therapeutics and identifying drug targets for chronic neuropathic pain.

Limitations of the study

Although our study established miR-323-3p targeting of Kv2.1 as significant in chronic neuropathic pain pathogenesis, Kv2.1 may not be its only downstream effector. RNA-seq data showed multiple downregulated miR-323-3p targets (*ATP11A*, *FMR1*, *GREM2*, and *VSNL1*) that could contribute to the alteration of the nociceptive response. Moreover, previous research also revealed that miR-323-3p might affect the expression of various genes.[13,15] Therefore, obtaining a comprehensive understanding of the role of miR-323-3p in sensory neurons will enhance our knowledge of neuropathic pain pathogenesis. In addition, it should be noted that most of our experiments were conducted on male rats. Interestingly, specific pathways in sensory macrophages and spinal microglia have been shown to be involved in the sexual dimorphism of neuropathic pain.[53,54] Notably, sexual dimorphism may be restricted to macrophages and/or microglia because the inhibition of pain-related signaling in neurons and astrocytes led to similar analgesic effects in both sexes.[55] The neuron-specific expression of antagomir-323 and Kv2.1 in TGs may account for the consistent pain phenotypes observed in both male and female rats.

RESOURCE AVAILABILITY

Lead contact

Requests for further information and resources should be directed to and will be fulfilled by the lead contact, Jin Tao (taoj@suda.edu.cn).

Materials availability

Reagents generated in this study are available from the lead contact upon request.

Data and code availability

- miRNA-seq and RNA-seq data are available in the National Center for Biotechnology Information Gene Expression Omnibus (GEO) with accession numbers GEO: GSE192803 and GSE224814, respectively. All study data are included in the article and/or supplemental information.
- No original code was developed in this study.
- Any additional information required to reanalyze the data reported in this paper is available from the lead contact upon reasonable request.

ACKNOWLEDGMENTS

This work was supported by grants from the National Science Foundation for Distinguished Young Scholars of China (82425019), the National Key Research and Development Program of China (2024YFC2510103), the National Natural Science Foundation of China (82271245, 82371218, and 82402888), the Natural Science Foundation of Jiangsu Province (BK20240304), the Youth Talent Project of Wuxi Health Commission (Q202343), the Jiangsu Key Laboratory of Drug Discovery and Translational Research for Brain Diseases, and the Priority Academic Program Development of Jiangsu Higher Education Institutions.

AUTHOR CONTRIBUTIONS

J.T. conceptualized the idea and supervised the project. R.Q., Y.T., S.W., Y.Z., Y.R., and J.T. designed the research; R.Q., Y.T., S.W., Y.Z., Y.S., D.J., Z.H., G. C., G.Z., and Y.Z. performed the research; R.Q., Y.T., Y.Z., and S.W. analyzed the data; and R.Q., D.J., Y.Z., and J.T. wrote the paper. All authors revised the article critically for intellectual content and have read and approved the final manuscript.

DECLARATION OF INTERESTS

The authors have no competing interests to declare.

STAR★METHODS

Detailed methods are provided in the online version of this paper and include the following:

- KEY RESOURCES TABLE
- EXPERIMENTAL MODEL AND STUDY PARTICIPANT DETAILS
  - Animals
  - Cell lines
- METHOD DETAILS
  - Animal models
  - Behavioral tests
  - RNA sequencing (RNA-seq)
  - Drug administration
  - Immunohistochemistry
  - Western blot analysis
  - Luciferase reporter assay
  - Real-time quantitative PCR (RT–qPCR)
  - Fluorescence *in situ* hybridization (FISH)
  - Chromatin immunoprecipitation (ChIP)-qPCR assay
  - Preparation of dissociated TG neurons
  - Electrophysiology
- QUANTIFICATION AND STATISTICAL ANALYSIS

SUPPLEMENTAL INFORMATION

Supplemental information can be found online at https://doi.org/10.1016/j.celrep.2025.116016.

Received: November 15, 2024
Revised: May 7, 2025
Accepted: June 27, 2025

REFERENCES

1. Canavero, S., and Bonicalzi, V. (2003). Chronic neuropathic pain. N. Engl. J. Med. *348*, 2688–2689. https://doi.org/10.1056/NEJM200306263482617.
2. Cruccu, G., Di Stefano, G., and Truini, A. (2020). Trigeminal Neuralgia. N. Engl. J. Med. *383*, 754–762. https://doi.org/10.1056/NEJMra1914484.
3. Ghazisaeidi, S., Muley, M.M., and Salter, M.W. (2023). Neuropathic Pain: Mechanisms, Sex Differences, and Potential Therapies for a Global Problem. Annu. Rev. Pharmacol. Toxicol. *63*, 565–583. https://doi.org/10.1146/annurev-pharmtox-051421-112259.
4. Megat, S., Ray, P.R., Tavares-Ferreira, D., Moy, J.K., Sankaranarayanan, I., Wanghzou, A., Fang Lou, T., Barragan-Iglesias, P., Campbell, Z.T., Dussor, G., and Price, T.J. (2019). Differences between Dorsal Root and Trigeminal Ganglion Nociceptors in Mice Revealed by Translational Profiling. J. Neurosci. *39*, 6829–6847. https://doi.org/10.1523/JNEUROSCI.2663-18.2019.
5. Kogelman, L.J.A., Christensen, R.E., Pedersen, S.H., Bertalan, M., Hansen, T.F., Jansen-Olesen, I., and Olesen, J. (2017). Whole transcriptome expression of trigeminal ganglia compared to dorsal root ganglia in Rattus Norvegicus. Neuroscience *350*, 169–179. https://doi.org/10.1016/j.neuroscience.2017.03.027.
6. Korczeniewska, O.A., Katzmann Rider, G., Gajra, S., Narra, V., Ramavajla, V., Chang, Y.J., Tao, Y., Soteropoulos, P., Husain, S., Khan, J., et al. (2020). Differential gene expression changes in the dorsal root versus trigeminal ganglia following peripheral nerve injury in rats. Eur. J. Pain *24*, 967–982. https://doi.org/10.1002/ejp.1546.
7. Krol, J., Loedige, I., and Filipowicz, W. (2010). The widespread regulation of microRNA biogenesis, function and decay. Nat. Rev. Genet. *11*, 597–610. https://doi.org/10.1038/nrg2843.
8. Bartel, D.P. (2004). MicroRNAs: genomics, biogenesis, mechanism, and function. Cell *116*, 281–297. https://doi.org/10.1016/s0092-8674(04)00045-5.
9. Polli, A., Godderis, L., Ghosh, M., Ickmans, K., and Nijs, J. (2020). Epigenetic and miRNA Expression Changes in People with Pain: A Systematic Review. J. Pain *21*, 763–780. https://doi.org/10.1016/j.jpain.2019.12.002.
10. Garzon, R., Marcucci, G., and Croce, C.M. (2010). Targeting microRNAs in cancer: rationale, strategies and challenges. Nat. Rev. Drug Discov. *9*, 775–789. https://doi.org/10.1038/nrd3179.
11. Rupaimoole, R., and Slack, F.J. (2017). MicroRNA therapeutics: towards a new era for the management of cancer and other diseases. Nat. Rev. Drug Discov. *16*, 203–222. https://doi.org/10.1038/nrd.2016.246.
12. Yang, Q., Wei, B., Peng, C., Wang, L., and Li, C. (2022). Identification of serum exosomal miR-98-5p, miR-183-5p, miR-323-3p and miR-19b-3p as potential biomarkers for glioblastoma patients and investigation of their mechanisms. Curr. Res. Transl. Med. *70*, 103315. https://doi.org/10.1016/j.retram.2021.103315.
13. Shi, C.C., Pan, L.Y., Zhao, Y.Q., Li, Q., and Li, J.G. (2020). MicroRNA-323-3p inhibits oxidative stress and apoptosis after myocardial infarction by targeting TGF-beta2/JNK pathway. Eur. Rev. Med. Pharmacol. Sci. *24*, 6961–6970. https://doi.org/10.26355/eurrev_202006_21688.
14. Du, S., Shen, S., Ding, S., and Wang, L. (2021). Suppression of microRNA-323-3p restrains vascular endothelial cell apoptosis via promoting sirtuin-1 expression in coronary heart disease. Life Sci. *270*, 119065. https://doi.org/10.1016/j.lfs.2021.119065.
15. Fiori, L.M., Kos, A., Lin, R., Théroux, J.F., Lopez, J.P., Kühne, C., Eggert, C., Holzapfel, M., Huettl, R.E., Mechawar, N., et al. (2021). miR-323a regulates ERBB4 and is involved in depression. Mol. Psychiatry *26*, 4191–4204. https://doi.org/10.1038/s41380-020-00953-7.
16. Ren, K., and Dubner, R. (2010). Interactions between the immune and nervous systems in pain. Nat. Med. *16*, 1267–1276. https://doi.org/10.1038/nm.2234.
17. Spitz, F., and Furlong, E.E.M. (2012). Transcription factors: from enhancer binding to developmental control. Nat. Rev. Genet. *13*, 613–626. https://doi.org/10.1038/nrg3207.
18. Riccio, A. (2010). Dynamic epigenetic regulation in neurons: enzymes, stimuli and signaling pathways. Nat. Neurosci. *13*, 1330–1337. https://doi.org/10.1038/nn.2671.
19. Guccione, E., and Richard, S. (2019). The regulation, functions and clinical relevance of arginine methylation. Nat. Rev. Mol. Cell Biol. *20*, 642–657. https://doi.org/10.1038/s41580-019-0155-x.
20. Yang, Y., and Bedford, M.T. (2013). Protein arginine methyltransferases and cancer. Nat. Rev. Cancer *13*, 37–50. https://doi.org/10.1038/nrc3409.
21. Jambhekar, A., Dhall, A., and Shi, Y. (2019). Roles and regulation of histone methylation in animal development. Nat. Rev. Mol. Cell Biol. *20*, 625–641. https://doi.org/10.1038/s41580-019-0151-1.
22. Dong, F., Li, Q., Yang, C., Huo, D., Wang, X., Ai, C., Kong, Y., Sun, X., Wang, W., Zhou, Y., et al. (2018). PRMT2 links histone H3R8 asymmetric dimethylation to oncogenic activation and tumorigenesis of glioblastoma. Nat. Commun. *9*, 4552. https://doi.org/10.1038/s41467-018-06968-7.
23. Ambros, V. (2004). The functions of animal microRNAs. Nature *431*, 350–355. https://doi.org/10.1038/nature02871.
24. Sanders, L.N., Schoenhard, J.A., Saleh, M.A., Mukherjee, A., Ryzhov, S., McMaster, W.G., Jr., Nolan, K., Gumina, R.J., Thompson, T.B., Magnuson, M.A., et al. (2016). BMP Antagonist Gremlin 2 Limits Inflammation After Myocardial Infarction. Circ. Res. *119*, 434–449. https://doi.org/10.1161/circresaha.116.308700.
25. Sun, Z.W., Waybright, J.M., Beldar, S., Chen, L., Foley, C.A., Norris-Drouin, J.L., Lyu, T.J., Dong, A., Min, J., Wang, Y.P., et al. (2022). Cdyl Deficiency Brakes Neuronal Excitability and Nociception through Promoting Kcnb1 Transcription in Peripheral Sensory Neurons. Adv. Sci. *9*, e2104317. https://doi.org/10.1002/advs.202104317.
26. Braunewell, K.H., Dwary, A.D., Richter, F., Trappe, K., Zhao, C., Giegling, I., Schönrath, K., and Rujescu, D. (2011). Association of VSNL1 with schizophrenia, frontal cortical function, and biological significance for its gene product as a modulator of cAMP levels and neuronal morphology. Transl. Psychiatry *1*, e22. https://doi.org/10.1038/tp.2011.20.
27. Segawa, K., Kikuchi, A., Noji, T., Sugiura, Y., Hiraga, K., Suzuki, C., Haginoya, K., Kobayashi, Y., Matsunaga, M., Ochiai, Y., et al. (2021). A sublethal ATP11A mutation associated with neurological deterioration causes aberrant phosphatidylcholine flipping in plasma membranes. J. Clin. Investig. *131*, e148005. https://doi.org/10.1172/jci148005.
28. Price, T.J., Rashid, M.H., Millecamps, M., Sanoja, R., Entrena, J.M., and Cervero, F. (2007). Decreased nociceptive sensitization in mice lacking the fragile X mental retardation protein: role of mGluR1/5 and mTOR. J. Neurosci. *27*, 13958–13967. https://doi.org/10.1523/jneurosci.4383-07.2007.
29. Mohapatra, D.P., Misonou, H., Pan, S.J., Held, J.E., Surmeier, D.J., and Trimmer, J.S. (2009). Regulation of intrinsic excitability in hippocampal neurons by activity-dependent modulation of the KV2.1 potassium channel. Channels *3*, 46–56. https://doi.org/10.4161/chan.3.1.7655.
30. Bartel, D.P. (2009). MicroRNAs: target recognition and regulatory functions. Cell *136*, 215–233. https://doi.org/10.1016/j.cell.2009.01.002.
31. Sakai, A., Saitow, F., Miyake, N., Miyake, K., Shimada, T., and Suzuki, H. (2013). miR-7a alleviates the maintenance of neuropathic pain through regulation of neuronal excitability. Brain *136*, 2738–2750. https://doi.org/10.1093/brain/awt191.
32. Favereaux, A., Thoumine, O., Bouali-Benazzouz, R., Roques, V., Papon, M.A., Salam, S.A., Drutel, G., Léger, C., Calas, A., Nagy, F., and Landry, M. (2011). Bidirectional integrative regulation of Cav1.2 calcium channel by microRNA miR-103: role in pain. EMBO J. *30*, 3830–3841. emboj2011249.
33. Pan, Z., Zhang, M., Ma, T., Xue, Z.Y., Li, G.F., Hao, L.Y., Zhu, L.J., Li, Y.Q., Ding, H.L., and Cao, J.L. (2016). Hydroxymethylation of microRNA-365-3p

Regulates Nociceptive Behaviors via Kcnh2. J. Neurosci. *36*, 2769–2781. https://doi.org/10.1523/JNEUROSCI.3474-15.2016.

34. Peng, C., Li, L., Zhang, M.D., Bengtsson Gonzales, C., Parisien, M., Belfer, I., Usoskin, D., Abdo, H., Furlan, A., Häring, M., et al. (2017). miR-183 cluster scales mechanical pain sensitivity by regulating basal and neuropathic pain genes. Science *356*, 1168–1171. https://doi.org/10.1126/science.aam7671.
35. Venkatesh, S., and Workman, J.L. (2015). Histone exchange, chromatin structure and the regulation of transcription. Nat. Rev. Mol. Cell Biol. *16*, 178–189. https://doi.org/10.1038/nrm3941.
36. Yin, Y., Morgunova, E., Jolma, A., Kaasinen, E., Sahu, B., Khund-Sayeed, S., Das, P.K., Kivioja, T., Dave, K., Zhong, F., et al. (2017). Impact of cytosine methylation on DNA binding specificities of human transcription factors. Science *356*, eaaj2239. https://doi.org/10.1126/science.aaj2239.
37. Pan, Z., Zhu, L.J., Li, Y.Q., Hao, L.Y., Yin, C., Yang, J.X., Guo, Y., Zhang, S., Hua, L., Xue, Z.Y., et al. (2014). Epigenetic modification of spinal miR-219 expression regulates chronic inflammation pain by targeting CaMKII-gamma. J. Neurosci. *34*, 9476–9483. https://doi.org/10.1523/JNEUROSCI.5346-13.2014.
38. Iwasaki, H., Kovacic, J.C., Olive, M., Beers, J.K., Yoshimoto, T., Crook, M. F., Tonelli, L.H., and Nabel, E.G. (2010). Disruption of protein arginine N-methyltransferase 2 regulates leptin signaling and produces leanness in vivo through loss of STAT3 methylation. Circ. Res. *107*, 992–1001. https://doi.org/10.1161/CIRCRESAHA.110.225326.
39. Xu, Z., Xie, W., Feng, Y., Wang, Y., Li, X., Liu, J., Xiong, Y., He, Y., Chen, L., Liu, G., and Wu, Q. (2022). Positive interaction between GPER and beta-alanine in the dorsal root ganglion uncovers potential mechanisms: mediating continuous neuronal sensitization and neuroinflammation responses in neuropathic pain. J. Neuroinflammation *19*, 164. https://doi.org/10.1186/s12974-022-02524-9.
40. Nie, H., Liu, B., Yin, C., Chen, R., Wang, J., Zeng, D., Tai, Y., Xie, J., He, D., and Liu, B. (2021). Gene Expression Profiling of Contralateral Dorsal Root Ganglia Associated with Mirror-Image Pain in a Rat Model of Complex Regional Pain Syndrome Type-I. J. Pain Res. *14*, 2739–2756. https://doi.org/10.2147/JPR.S322372.
41. Dong, T., Si, H., Li, Z., Bai, Q., and Tao, F. (2022). Transcriptomic Analysis of Trigeminal Ganglion and Spinal Trigeminal Nucleus Caudalis in Mice with Inflammatory Temporomandibular Joint Pain. J. Pain Res. *15*, 1487–1502. https://doi.org/10.2147/JPR.S364887.
42. Wu, C., Shang, H.F., Wang, Y.J., Wang, J.H., Zuo, Z.X., Lian, Y.N., Liu, L., Zhang, C., and Li, X.Y. (2023). Cingulate protein arginine methyltransferases 1 regulates peripheral hypersensitivity via fragile X messenger ribonucleoprotein. Front. Mol. Neurosci. *16*, 1153870. https://doi.org/10.3389/fnmol.2023.1153870.
43. Ahlstrom, F.H.G., Matlik, K., Viisanen, H., Blomqvist, K.J., Liu, X., Lilius, T. O., Sidorova, Y., Kalso, E.A., and Rauhala, P.V. (2021). Spared Nerve Injury Causes Sexually Dimorphic Mechanical Allodynia and Differential Gene Expression in Spinal Cords and Dorsal Root Ganglia in Rats. Mol. Neurobiol. *58*, 5396–5419. https://doi.org/10.1007/s12035-021-02447-1.
44. Cuevas-Diaz Duran, R., Li, Y., Garza Carbajal, A., You, Y., Dessauer, C.W., Wu, J., and Walters, E.T. (2023). Major Differences in Transcriptional Alterations in Dorsal Root Ganglia Between Spinal Cord Injury and Peripheral Neuropathic Pain Models. J. Neurotrauma *40*, 883–900. https://doi.org/10.1089/neu.2022.0238.
45. Zhang, M., Xu, Y., Zhu, G., Zeng, Q., Gao, R., Qiu, J., Su, W., and Wang, R. (2024). Human C15orf39 Inhibits Inflammatory Response via PRMT2 in Human Microglial HMC3 Cell Line. Int. J. Mol. Sci. *25*, 6025. https://doi.org/10.3390/ijms25116025.
46. Busserolles, J., Tsantoulas, C., Eschalier, A., and López García, J.A. (2016). Potassium channels in neuropathic pain: advances, challenges, and emerging ideas. Pain *157*, S7–S14. https://doi.org/10.1097/j.pain.0000000000000368.
47. Chien, L.Y., Cheng, J.K., Chu, D., Cheng, C.F., and Tsaur, M.L. (2007). Reduced expression of A-type potassium channels in primary sensory neurons induces mechanical hypersensitivity. J. Neurosci. *27*, 9855–9865. https://doi.org/10.1523/JNEUROSCI.0604-07.2007.
48. Roza, C., and Lopez-Garcia, J.A. (2008). Retigabine, the specific KCNQ channel opener, blocks ectopic discharges in axotomized sensory fibres. Pain *138*, 537–545. https://doi.org/10.1016/j.pain.2008.01.031.
49. Murakoshi, H., and Trimmer, J.S. (1999). Identification of the Kv2.1 K+ channel as a major component of the delayed rectifier K+ current in rat hippocampal neurons. J. Neurosci. *19*, 1728–1735. https://doi.org/10.1523/JNEUROSCI.19-05-01728.1999.
50. Tsantoulas, C., Zhu, L., Yip, P., Grist, J., Michael, G.J., and McMahon, S.B. (2014). Kv2 dysfunction after peripheral axotomy enhances sensory neuron responsiveness to sustained input. Exp. Neurol. *251*, 115–126. https://doi.org/10.1016/j.expneurol.2013.11.011.
51. Bhuiyan, S.A., Xu, M., Yang, L., Semizoglou, E., Bhatia, P., Pantaleo, K.I., Tochitsky, I., Jain, A., Erdogan, B., Blair, S., et al. (2024). Harmonized cross-species cell atlases of trigeminal and dorsal root ganglia. Sci. Adv. *10*, eadj9173. https://doi.org/10.1126/sciadv.adj9173.
52. Everill, B., and Kocsis, J.D. (2000). Nerve growth factor maintains potassium conductance after nerve injury in adult cutaneous afferent dorsal root ganglion neurons. Neuroscience *100*, 417–422. https://doi.org/10.1016/s0306-4522(00)00263-3.
53. Luo, X., Huh, Y., Bang, S., He, Q., Zhang, L., Matsuda, M., and Ji, R.R. (2019). Macrophage Toll-like Receptor 9 Contributes to Chemotherapy-Induced Neuropathic Pain in Male Mice. J. Neurosci. *39*, 6848–6864. https://doi.org/10.1523/jneurosci.3257-18.2019.
54. Midavaine, É., Côté, J., Marchand, S., and Sarret, P. (2021). Glial and neuroimmune cell choreography in sexually dimorphic pain signaling. Neurosci. Biobehav. Rev. *125*, 168–192. https://doi.org/10.1016/j.neubiorev.2021.01.023.
55. Chen, G., Luo, X., Qadri, M.Y., Berta, T., and Ji, R.R. (2018). Sex-Dependent Glial Signaling in Pathological Pain: Distinct Roles of Spinal Microglia and Astrocytes. Neurosci. Bull. *34*, 98–108. https://doi.org/10.1007/s12264-017-0145-y.
56. Sun, Y., Tao, Y., Cao, J., Zhang, Y., Huang, Z., Wang, S., Lu, W., Zhu, Q., Shan, L., Jiang, D., et al. (2025). H3K27 Trimethylation-Mediated Downregulation of miR-216a-3p in Sensory Neurons Regulates Neuropathic Pain Behaviors via Targeting STIM1. J. Neurosci. *45*, e0607242024. https://doi.org/10.1523/jneurosci.0607-24.2024.
57. Qi, R., Cao, J., Sun, Y., Li, Y., Huang, Z., Jiang, D., Jiang, X.H., Snutch, T. P., Zhang, Y., and Tao, J. (2022). Histone methylation-mediated microRNA-32-5p down-regulation in sensory neurons regulates pain behaviors via targeting Cav3.2 channels. Proc. Natl. Acad. Sci. USA *119*, e2117209119. https://doi.org/10.1073/pnas.2117209119.
58. Martin, Y.B., and Avendano, C. (2009). Effects of removal of dietary polyunsaturated fatty acids on plasma extravasation and mechanical allodynia in a trigeminal neuropathic pain model. Mol. Pain *5*, 8. https://doi.org/10.1186/1744-8069-5-8.
59. Li, Q.Y., Chen, S.X., Liu, J.Y., Yao, P.W., Duan, Y.W., Li, Y.Y., and Zang, Y. (2022). Neuroinflammation in the anterior cingulate cortex: the potential supraspinal mechanism underlying the mirror-image pain following motor fiber injury. J. Neuroinflammation *19*, 162. https://doi.org/10.1186/s12974-022-02525-8.
60. Wang, H., Wei, Y., Pu, Y., Jiang, D., Jiang, X., Zhang, Y., and Tao, J. (2019). Brain-derived neurotrophic factor stimulation of T-type Ca(2+) channels in sensory neurons contributes to increased peripheral pain sensitivity. Sci. Signal. *12*, eaaw2300. https://doi.org/10.1126/scisignal.aaw2300.
61. Zhang, Y., Qian, Z., Jiang, D., Sun, Y., Gao, S., Jiang, X., Wang, H., and Tao, J. (2021). Neuromedin B receptor stimulation of Cav3.2 T-type Ca(2+) channels in primary sensory neurons mediates peripheral pain hypersensitivity. Theranostics *11*, 9342–9357. https://doi.org/10.7150/thno.62255.
62. Vos, B.P., Strassman, A.M., and Maciewicz, R.J. (1994). Behavioral evidence of trigeminal neuropathic pain following chronic constriction injury

to the rat's infraorbital nerve. J. Neurosci. *14*, 2708–2723. https://doi.org/10.1523/jneurosci.14-05-02708.1994.

63. Dixon, W.J. (1980). Efficient analysis of experimental observations. Annu. Rev. Pharmacol. Toxicol. *20*, 441–462. https://doi.org/10.1146/annurev.pa.20.040180.002301.

64. Huang, Z., Zhang, Y., Wang, S., Qi, R., Tao, Y., Sun, Y., Jiang, D., Jiang, X., and Tao, J. (2024). FOXD3-mediated transactivation of ALKBH5 promotes neuropathic pain via m(6)A-dependent stabilization of 5-HT3A mRNA in sensory neurons. Proc. Natl. Acad. Sci. USA *121*, e2312861121. https://doi.org/10.1073/pnas.2312861121.

65. Tan, P.H., Gao, Y.J., Berta, T., Xu, Z.Z., and Ji, R.R. (2012). Short small-interfering RNAs produce interferon-alpha-mediated analgesia. Br. J. Anaesth. *108*, 662–669. https://doi.org/10.1093/bja/aer492.

66. Zhao, X., Zhang, Y., Qin, W., Cao, J., Zhang, Y., Ni, J., Sun, Y., Jiang, X., and Tao, J. (2016). Serotonin type-1D receptor stimulation of A-type K(+) channel decreases membrane excitability through the protein kinase A- and B-Raf-dependent p38 MAPK pathways in mouse trigeminal ganglion neurons. Cell. Signal. *28*, 979–988. https://doi.org/10.1016/j.cellsig.2016.05.004.

67. Zhang, Y., Wang, H., Sun, Y., Huang, Z., Tao, Y., Wang, Y., Jiang, X., and Tao, J. (2023). Trace amine-associated receptor 1 regulation of Kv1.4 channels in trigeminal ganglion neurons contributes to nociceptive behaviors. J. Headache Pain *24*, 49. https://doi.org/10.1186/s10194-023-01582-5.

68. Wang, Y., Wang, X., Qi, R., Lu, Y., Tao, Y., Jiang, D., Sun, Y., Jiang, X., Liu, C., Zhang, Y., and Tao, J. (2022). Interleukin 33-mediated inhibition of A-type K(+) channels induces sensory neuronal hyperexcitability and nociceptive behaviors in mice. Theranostics *12*, 2232–2247. https://doi.org/10.7150/thno.69320.

69. Zhang, Y., Li, H., Pu, Y., Gong, S., Liu, C., Jiang, X., and Tao, J. (2015). Melatonin-mediated inhibition of Purkinje neuron P-type Ca(2)(+) channels in vitro induces neuronal hyperexcitability through the phosphatidylinositol 3-kinase-dependent protein kinase C delta pathway. J. Pineal Res. *58*, 321–334. https://doi.org/10.1111/jpi.12218.

70. Cao, J., Zhang, Y., Wu, L., Shan, L., Sun, Y., Jiang, X., and Tao, J. (2019). Electrical stimulation of the superior sagittal sinus suppresses A-type K(+) currents and increases P/Q- and T-type Ca(2+) currents in rat trigeminal ganglion neurons. J. Headache Pain *20*, 87. https://doi.org/10.1186/s10194-019-1037-5.

STAR★METHODS

KEY RESOURCES TABLE

REAGENT or RESOURCE	SOURCE	IDENTIFIER
Antibodies		
Rabbit monoclonal anti-FOXA2	Cell Signaling Technology	CAT# 8186; RRID: AB_10891055
Rabbit polyclonal anti-H3R8me2a	Active Motif	CAT# 39651; RRID: AB_2793290
Rabbit polyclonal anti-Kv2.1	Proteintech	CAT# 19963-1-AP; RRID: AB_2878631
Mouse monoclonal anti-Kv2.1	Abcam	CAT# ab192761; RRID: AB_3677394
Mouse monoclonal anti-NeuN	Merck Millipore	CAT# MAB377; RRID: AB_2298772
Mouse monoclonal anti-GS	Abcam	CAT# ab64613; RRID: AB_1140869
Mouse monoclonal anti-CGRP	Abcam	CAT# ab81887; RRID: AB_1658411
Mouse monoclonal anti-NF200	Abcam	CAT# ab215903; RRID: AB_3107022
Rabbit polyclonal anti-GAPDH	Proteintech	CAT# 10494-1-AP; RRID: AB_2263076
Rabbit polyclonal anti-H3	Abcam	CAT# ab61251; RRID: AB_941952
Rabbit polyclonal anti-PRMT2	Active Motif	CAT# 61419; RRID: AB_2793656
goat anti-rabbit IgG-HRP secondary antibody	R&D Systems	CAT# HAF008; RRID: AB_357235
goat anti-mouse IgG-HRP secondary antibody	R&D Systems	CAT# BAF007; RRID: AB_355776
Goat anti-Rabbit IgG (H + L) secondary antibody, Alexa Fluor 555	Cell Signaling Technology	CAT# 4413s; RRID: AB_10694110
Goat anti-Rabbit IgG (H + L) secondary antibody, Alexa Fluor 488	Cell Signaling Technology	CAT# 4412s; RRID: AB_1904025
Goat anti-Mouse IgG (H + L) secondary antibody, Alexa Fluor 555	Cell Signaling Technology	CAT# 4409s; RRID: AB_1904022
Goat anti-Mouse IgG (H + L) secondary antibody, Alexa Fluor 488	Cell Signaling Technology	CAT# 4408s; RRID: AB_10694704
Chemicals, peptides, and recombinant proteins		
Kv2.1 Blocking Peptide	Alomone	CAT# BLP-PC012 -40ug
DAPI	Thermo Fisher Scientific	CAT# 62248
IB4	Sigma-Aldrich	CAT# L2895
Protease Inhibitor Cocktail	Cell Signaling Technology	CAT# 7012L
PVDF Membrane	Merck Millipore	CAT# ipvh00010
Lipofectamine 6000	Beyotime	CAT# C0526FT
DMEM	Gibco	CAT# C11330500BT
Trizol	Takara	CAT# 9109
Kv2 inhibitor Guangxitoxin-1E	Tocris	CAT# 5676/100U
Potassium Chloride	Sigma-Aldrich	CAT# P5405-250G
Calcium Chloride	Sigma-Aldrich	CAT# C5670-100G

(*Continued on next page*)

Continued

REAGENT or RESOURCE	SOURCE	IDENTIFIER
Magnesium Chloride	Sigma-Aldrich	CAT# M4880-100G
EGTA	Sigma-Aldrich	CAT# E0396-10G/E4378-10G
HEPES	Sigma-Aldrich	CAT# H4034-100G
Na-GTP	Sigma-Aldrich	CAT# G8877-250MG
Mg-ATP	Sigma-Aldrich	CAT# A9187-500MG
Choline Chloride	Sigma-Aldrich	CAT# C1879-500G
Glucose	Sigma-Aldrich	CAT# G7021-1KG
DiI	Thermo Fisher Scientific	CAT# D282
Collagenase	Sigma-Aldrich	CAT# 11088866001
Trypsin	Sigma-Aldrich	CAT# T1426-100MG
Critical commercial assays		
SimpleChIP(R) Plus Kit (Magnetic Bead)	Cell Signaling Technology	CAT# 9005
SYBR Green qPCR Master Mix	Bimake	CAT# B21703
PrimeScript RT Master Mix	Takara	CAT# RR036A
Dual-Luciferase Reporter Assay System	Promega	CAT# E1910
Pierce BCA Protein Assay	Thermo Fisher Scientific	CAT# A65453
Deposited data		
miRNA-seq	Sun et al. [56]	GSE192803
RNA-seq	This paper	GSE224814
Experimental models: Cell lines		
PC12	Pricella	CAT# CL-0480
Experimental models: Organisms/strains		
Sprague-Dawley rats	Shanghai SLAC Laboratory	N/A
Oligonucleotides		
Agomir, antagomir, siRNAs, and probes sequences are listed in Table S1	This paper	N/A
Primers for miRNAs are listed in Table S2	This paper	N/A
Sequences of nucleotides are listed in Table S3	This paper	N/A
Software and algorithms		
Prism 8.0	GraphPad	https://www.graphpad.com
Quantity One software	Bio-Rad Laboratories	https://www.bio-rad.com/
pClamp10 and Clampfit 10.2	Molecular Devices	https://www.moleculardevices.com/

EXPERIMENTAL MODEL AND STUDY PARTICIPANT DETAILS

Animals

The animals used in the study were obtained from Shanghai SLAC Laboratory Animal Co., Ltd. and housed at the Animal Facility of Soochow University. The Animal Care and Use Committee of Soochow University approved all animal procedures, and the protocols adhered to the guidelines established by the National Institutes of Health (NIH) for animal research, as well as the International Association for the Study of Pain. Wild-type adult Sprague–Dawley (SD) rats weighing 180–220 g were kept in cages with soft bedding. All animal studies were performed in male rats unless otherwise indicated in the present study. They were maintained in facilities with controlled temperature and humidity, following a 12/12-h light-dark cycle. The rats had *ad libitum* access to food and water. Efforts were taken to minimize animal suffering and the number of animals used.

Cell lines

Two cell lines were used in this study: Human embryonic kidney 293 (HEK293) cells and rat pheochromocytoma (PC12) cells were purchased from Cell Bank of Type Culture Collection of the Chinese Academy of Sciences (Shanghai Institute of Cell Biology), and have been authenticated. Cells were cultured in DMEM with 10% FBS. Transfections were performed with Lipofectamine 6000 (Beyotime) for HEK293 and PC12 cells according to the manufacturer's instructions. Cells were not mycoplasma positive, and all DNA plasmids were cleared of endotoxin.

METHOD DETAILS

Animal models

As previously described,[57,58] chronic constriction injury (CCI) of the infraorbital nerve (ION) was utilized to establish an animal model of trigeminal neuropathic pain. In brief, during the surgical procedures, the rats were deeply anesthetized using isoflurane. An approximately 1 cm long incision was made along the gingivobuccal margin. The incision started just proximal to the left upper first molar. ION was carefully separated with a blunt curved glass rod, and two ligatures were tied loosely around the ION with 4–0 chromic gut sutures (approximately 2 mm apart). The IONs of sham animals were exposed using the same surgical procedure without ligation. To produce a spared nerve injury (SNI) model, the biceps femoris muscle of rats was dissected to expose the three terminal branches of the sciatic nerve as described previously.[59] The common peroneal and the tibial nerves were ligated with 5-0 silk and sectioned distal to the ligation, removing 2–4 mm of the distal nerve stump. For the sham procedure, three peripheral branches of the sciatic nerve were similarly exposed without damage. Chronic inflammatory pain was induced by subcutaneous injection of CFA (20 μL) into the unilateral buccal pad as described previously.[60] The control group received the same volume of sterile saline injections.

Behavioral tests

During the behavioral experiments, the investigators responsible for conducting the tests were blinded to the treatment groups. Orofacial behavioral tests were conducted one day prior to any surgeries and at predetermined intervals thereafter, as described previously.[57,60,61] Each rat was placed in a plastic cage individually, allowing for a 2-h adaptation period before testing commenced. Stimuli were applied to the orofacial skin near the center of the left vibrissal pad. A series of *von* Frey filaments (Stoelting) was used, starting from 0.008 g and gradually increasing up to 15 g. These filaments were applied consecutively, at least 3 times with 2-s intervals, following the methodology established in previous studies.[57,60,61] To prevent tissue damage and excessive mechanical force, the 15 g filament was the highest gauge used. The escape threshold was determined by assessing the response to each *von* Frey filament. Positive nociceptive behavior, as described by Vos et al.[62] and in previous studies,[57] included attack/evasion responses and/or brisk withdrawal of the head. The minimal force needed to elicit positive nociceptive behavior was defined as the mechanical escape threshold. For testing mechanical sensitivity of SNI rats, animals were put in a plastic box (11 × 13 × 24 cm) on an elevated metal mesh floor and allowed 30 min for habituation. Mechanical pain sensitivity was determined by measuring paw withdrawal threshold (PWT) of rats via *von* Frey filaments. The 50% withdrawal threshold was determined using the up-down method of Dixon.[63]

RNA sequencing (RNA-seq)

mRNA sequencing service was provided by RiboBio Biological Technology (Guangzhou, China). Briefly, total RNA from rat TG tissues on day 14 after CCI-ION operation or sham operation was extracted with Trizol (Invitrogen, Carlsbad, CA, USA), and subjected to mRNA isolation using GenSeq mRNA Purification Kit (GenSeq, Inc., Shanghai, China). Then, the purified mRNA was used for library construction with GenSeq Directional RNA Library Prep Kit (GenSeq, Inc., Shanghai, China) by following manufacturer's recommendations. The mRNA was fragmented into ~300 nt in length. The first-strand cDNA was synthesized from the RNA fragments by reverse transcriptase and random hexamer primers, and the second-strand cDNA was synthesized in 2nd Strand Synthesis Buffer with dUTP Mix. Then, the double stranded cDNA fragments were subjected to end-repair and dAtailing, followed by adapter ligation. The adapter-ligated DNA samples were PCR amplified and purified to obtain sequencing libraries. Finally, the libraries were sequenced with sequencer on the paired-end 150 bp mode.

The miRNA sequencing data reported in this paper was generated from our published dataset,[56] and have been deposited in GEO under accession number GSE192803.

Drug administration

A percutaneous approach for injecting the trigeminal ganglion (intra-TG injection) was used as described previously.[57,64] In brief, a microinjection needle was inserted through the infraorbital foramen (IOF), infraorbital canal (IOC) and foramen rotundum. The needle tip terminated at the medial part of the TG. A 3 μL microinjection was slowly delivered (over 5 min), with 10 min of needle retention before the needle was removed. For intrathecal (*i.t.*) injection, a midline incision was made at the L4–L6 spinal level, muscles were gently pulled aside to visualize the caudal edge of L4–L6 vertebra, and a 26-gauge needle connected to a 10-μL microinjection syringe was implanted.[65] The tail-flick reflex was considered to be an indicator of the accuracy of each injection. The volume of intrathecal injection was 5 μL for each animal. 5′-Cholesteryl- and 2′-O-methyl-modified small interfering RNAs (siRNAs) specific for PRMT2 (PRMT2-siRNA), agomir-323-3p, antagomir-323-3p and the corresponding negative controls (GenePharma) were labeled with 6-carboxyfluorescein. The 5′-Cholesteryl-modification aimed to improve the delivery efficiency and the stability of the siRNA in systemic circulation. The 2′-O-methyl-modification significantly reduced off-target effects and immunostimulatory effects, and enhanced the nuclease stability of the siRNA. The siRNAs were intra-TG injected once daily for 2 consecutive days. The human synapsin 1 (hSyn) promoter confers highly neuron-specific gene expression. All of the recombinant lentiviral vectors containing the EGFP gene, including lenti-hSyn-miR-323-3p-up (miR-323-up), lenti-hSyn-miR-323-3p-antisense (miR-323-AS), and lenti-hSyn-Kv2.1-up (Kv2.1-up), were obtained from GenePharma. The virus titer used in this study was greater than 1×10^8 TU. The antagomir sequences

were blasted against the rat GenBank (https://blast.ncbi.nlm.nih.gov/) to exclude the presence of multiple target sequences in the rat genome. The specific sequences for the agomir, antagomir, siRNA, and shRNA are summarized in Table S1.

Immunohistochemistry

Immunohistochemistry was carried out as described in our previous studies.[60,66,67] In brief, fixed TGs were embedded in OCT and sectioned with a cryostat (Leica) at a 12-μm thickness. After washing, the tissue sections were blocked for 1 h with PBS containing 0.25% Triton X-100 and 5% normal goat serum. Subsequently, the TG sections were incubated at 4°C overnight with the following antibodies: anti-FOXA2 (rabbit, 1:200, Cell Signaling Technology), anti-H3R8me2a (rabbit, 1:200, Active Motif), anti-Kv2.1 (rabbit, 1:200, Proteintech), anti-NeuN (mouse, 1:400, Merck Millipore), anti-GS (mouse, 1:200, Abcam), anti-CGRP (mouse, 1:1000, Abcam), anti-NF200 (mouse, 1:400, Abcam), and anti-IB4 (5 μg/mL, Sigma–Aldrich). The sections were then incubated with appropriate Alexa Fluor 555- or Alexa Fluor 488-conjugated secondary antibodies (1:300, Cell Signaling Technology). After mounting with glycerin or DAPI solution, the sections were examined under an upright Nikon-104C fluorescence microscope, and images were captured with a CoolSNAP HQ2 charge-coupled device camera (Photometrics). Pre-incubation of the Kv2.1 antibody with its corresponding recombinant blocking peptide abolished the detection of Kv2.1 in TGs by immunofluorescence assays, ensuring the high specificity of the Kv2.1 antibody used in this study (Figure S10).

Western blot analysis

Western blot analysis was carried out as described previously.[60,68,69] Briefly, TG tissues from rats were lysed on ice for 30 min with RIPA lysis buffer (Beyotime Biotechnology). The protein concentration was measured using a BCA assay (Thermo Fisher Scientific). Equal amounts of total protein (30 μg) from each lysate were loaded and separated by SDS–PAGE prior to transfer onto a polyvinylidene fluoride membrane (Millipore). The membranes were blocked with TBS containing 5% nonfat milk for 1 h prior to incubation with primary antibodies against FOXA2 (rabbit, 1:1000, Cell Signaling Technology), GAPDH (rabbit, 1:10000, Proteintech), H3R8me2a (rabbit, 1:1000, Active Motif), H3 (rabbit, 1:1000, Abcam), PRMT2 (rabbit, 1:1000, Proteintech), and Kv2.1 (mouse, 1:1000, Abcam) at 4°C overnight. The membrane was washed and then incubated with a horseradish peroxidase-conjugated goat anti-rabbit secondary antibody (1:8000, R&D Systems). The protein bands were detected with Pierce ECL Western Blotting Substrate (Thermo Fisher Scientific). The ChemiDoc XRS system (Bio-Rad Laboratories) was used to capture images, and Quantity One software was used to analyze the protein band densities. GAPDH or H3 was used as the loading control. All unedited blot images are provided in the Data S1.

Luciferase reporter assay

A series of plasmids were generated by amplifying different truncations of the miR-323-3p promoter (S1 to S5) using specific primers. Each truncation fragment was then individually cloned and inserted into the pGL3-Basic (Promega) vector. Bioinformatic analyses including the JASPAR database (http://jaspar.genereg.net/) and the AliBaba2.1 (http://gene-regulation.com/pub/programs/alibaba2/) were utilized to explore the potential binding sequences of transcription factors, including FOXA2, AP1, and NFATC2, in the 431-bp region (ΔS, bp −443 to bp −13) of the *miR-323-3p* promoter. Sequences of the *miR-323-3p* promoter containing mutations in the binding site for FOXA2 (mut-FOXA2), AP1 (mut-AP1), or NFATC2 (mut-NFATC2) were cloned and inserted into the pGL3-Basic luciferase reporter plasmid. Full-length ΔS derived from the *miR-323-3p* promoter (miR-323-WT) was used as a control. Plasmids containing the firefly luciferase sequence, positioned upstream of either the wild-type 3′-UTR of KCNB1 (Kv2.1-wt) or the mutant 3′-UTR of KCNB1 (Kv2.1-mut), were cloned and inserted into pGL3 vectors. Sanger sequencing was applied to confirm all wild-type and mutant constructs. Furthermore, the Renilla luciferase vector pGMR-TK (Promega) was cotransfected with the pGL3 vector to enable data normalization during subsequent analyses. Kv2.1-wt, Kv2.1-mut, the miR-323-3p mimic (or its negative control), and pGMR-TK were transfected into HEK293T cells using Lipofectamine (Thermo Fisher Scientific). Similarly, plasmids containing mut-AP1, mut-FOXA2, mut-NFATC2, miR-323-wt and pGMR-TK were transfected into PC12 cells. After transfection, firefly and Renilla luciferase activities were assessed consecutively using the Dual-Glo Luciferase System (Promega) using a luminometer (TD-20/20, Turner BioSystems). All experiments were conducted in triplicate and repeated at least three times. Relative firefly luciferase activity was obtained by normalizing firefly luciferase activity against Renilla luciferase activity.

Real-time quantitative PCR (RT–qPCR)

In this study, total RNA was extracted from rat TG or PC12 cells using the Takara RNAiso Plus kit, following a previous protocol,[57] and was reverse-transcribed into cDNA using the PrimeScript RT Reagent Kit from Takara. For quantitative PCR (qPCR), the Roche LightCycler 96 System and SYBR Green qPCR Master Mix from Takara were utilized. The quantification of miRNA expression was performed using the $2^{-\Delta\Delta Cq}$ method, with U6 serving as the internal control for normalization. For the calculation of relative mRNA expression, the $2^{-\Delta\Delta Cq}$ method was employed, with GAPDH utilized as the normalization control. To ensure the specificity of the amplified PCR product, agarose gel electrophoresis and melt curve analysis were conducted. Each experiment was conducted with at least three biological replicates. The specific primers used for reverse transcription and qPCR are included in Tables S2 and S3, respectively. All unedited gel images are provided in the Data S1.

Fluorescence *in situ* hybridization (FISH)

As described previously,[57] the hybridization process was carried out with a FISH Kit (Exon Co., Guangzhou). Briefly, TG sections were treated with permeabilization buffer for 20 min. Then, 3% H_2O_2 was added dropwise to the tissue sections, which were incubated at room temperature for 15 min. A digoxin-labeled LNA detection probe specific for rno-miR-323-3p (5′-AGAGGTCGACCGTGTAATGTG-3′) and the corresponding negative control probe were denatured at 85°C and immediately chilled on ice. A scrambled locked nucleic acid (LNA) probe, which did not produce any fluorescent labeling, was employed as a negative control for the FISH analysis of TG sections (Figure S11). Following incubation with the denatured hybridization probe, TG sections were subjected to blocking with a 1% BSA solution in DEPC-treated PBS buffer and then exposed to a diluted Alexa Fluor 555-conjugated anti-digoxin antibody (1:300, Guangzhou Exon Technology). To perform FISH in combination with immunofluorescence staining, the sections underwent further processing involving immunostaining with specific antibodies targeting NeuN (mouse, 1:400, Merck Millipore), GS (mouse, 1:200, Abcam), FOXA2 (rabbit, 1:200, Cell Signaling Technology), H3R8me2a (rabbit, 1:200, Active Motif), and Kv2.1 (mouse, 1:200, Abcam). Subsequently, the sections were washed in PBS and incubated with Alexa Fluor 488-conjugated goat anti-rabbit/mouse IgG (1:400, Cell Signaling Technology). Finally, after staining with DAPI solution, the sections were observed and captured using a fluorescence microscope equipped with a CoolSNAP CCD camera (Photometrics HQ2).

Chromatin immunoprecipitation (ChIP)-qPCR assay

ChIP analysis in this study was carried out with a SimpleChIP Plus Enzymatic Chromatin IP Kit (Cell Signaling Technology) as described previously.[57] In brief, TG samples were subjected to crosslinking using 1% formaldehyde, and the crosslinking reaction was terminated by incubation with glycine. After two washes with PBS containing protease inhibitors, TG tissues were pelleted by centrifugation and resuspended in SDS lysis buffer. After incubation for 15 min, chromatin in the lysates was sonicated into fragments and centrifuged. Then, 10% of the supernatant was collected as input, and the rest of the supernatant was subjected to immunoprecipitation with 2 μg of an antibody against FOXA2 (Cell Signaling Technology), an antibody against H3R8me2a (Active Motif), or IgG (Santa Cruz) overnight at 4°C. Next, 30 μL of protein G magnetic beads was added to the mixture for incubation at 4°C for 2 h. After the protein-chromatin complexes were washed, they were eluted, and the crosslinks were reversed using proteinase K. The resulting DNA was then purified (Cell Signaling Technology) and collected for further analysis. To quantify the ChIP-enriched DNA, qPCR analysis was performed using specific primers designed for the FOXA2-binding sites (forward, 5′-CAGATTACTCAGTGCTTGGCTAT-3’; reverse, 5′-ATGCCGCTATGACTTCCAG-3′). The enrichment was normalized against the input samples. PCR products were separated and analyzed on agarose gels.

Preparation of dissociated TG neurons

TG neurons from rats were acutely dissociated following the protocol described in our previous studies.[57,70] In brief, rats were decapitated under anesthesia, and TGs were rapidly excised. After removal of connective tissue and trimming in ice-cold O_2-saturated DDB solution, the tissues were enzymatically digested by sequential incubation with 2.5 mg/mL collagenase D (Roche) at 37°C for 50 min and 2 mg/mL trypsin (Sigma) at 37°C for 15 min. Individual neurons were dissociated by gentle trituration of the ganglia using flame-polished Pasteur pipettes. Then, the cells were seeded in growth medium onto a glass coverslip coated with Matrigel (Merck) and incubated at 37°C in an incubator overnight. The following morning, the medium was replaced with fresh complete culture medium. Electrophysiological recordings were conducted within 24 h of cell isolation.

Electrophysiology

Recordings of TG neurons were performed at room temperature (22°C–24°C) as previously described.[57,60,68] The current measurements were performed using a MultiClamp 700B amplifier (Molecular Devices). The signals were filtered at a low-pass filter frequency of 2 kHz and digitized at a sampling rate of 10 kHz using a Digidata 1440 A digitizer (Molecular Devices). Data acquisition was carried out using pClamp10 software (Molecular Devices), and the collected data were subsequently analyzed using Clampfit 10.2 (Molecular Devices). The recording pipettes (World Precision Instruments) had a resistance of 3- to 5 megaohms when filled with internal solution. For voltage-gated K^+ channel (Kv) current recordings, the intracellular pipette solution contained (in mM) 140 KCl, 0.5 $CaCl_2$, 1 $MgCl_2$, 5 EGTA, 10 HEPES, 0.3 Na-GTP, and 3 Mg-ATP (pH 7.4 adjusted with KOH, 295 mOsm). The extracellular solution contained (in mM) 5 KCl, 1 $MgCl_2$, 0.03 $CaCl_2$, 150 choline-Cl, 10 HEPES, and 10 glucose (pH 7.4 adjusted with KOH, 310 mOsm). To obtain current-voltage (I-V) relationships, the membrane potential of neurons was held at −80 mV, and the neurons were stimulated with depolarizing voltage steps ranging from −70 to +70 mV in increments of 10 mV. Since Kv2.2 was not targeted by miR-323-3p, as validated by TargetScan and miRWalk (Figure S12), the Kv2.1 channel current was calculated by subtracting the Kv current recorded in the presence of the specific Kv2.1 channel blocker GxTX-1E (100 nM, Tocris) from the total Kv current. For current-clamp recordings, the intracellular pipette solution contained (in mM) 110 KCl, 25 HEPES, 10 NaCl, 0.3 Na-GTP, 4 Mg-ATP, and 2 EGTA (pH 7.4 adjusted with KOH, 295 mOsm). The extracellular solution contained (in mm) 128 NaCl, 2 KCl, 2 $CaCl_2$, 2 $MgCl_2$, 25 HEPES, and 30 glucose (pH 7.4 adjusted with NaOH, 305 mOsm). The established retrograde tracer DiI (20 mg/mL, Thermo Fisher) was subcutaneously injected into the whisker pads of rats. Four days after injection, small TG neurons (soma diameter <30 μm) were subjected to electrophysiological recording.

QUANTIFICATION AND STATISTICAL ANALYSIS

The data in the study are presented as the mean ± S.E.M. values. Two-tailed Student's *t* test was applied to detect the significance of differences between two groups. One-way ANOVA with the Bonferroni correction was used for multiple group comparisons. Comparisons involving multiple time points or multiple voltages were performed using a two-way ANOVA with the Bonferroni correction. Two-way repeated-measures (RM) ANOVA followed by the Bonferroni correction for multiple comparisons was applied to analyze the behavioral data. Differences with p values <0.05 were considered statistically significant.